12-19-2020

Quantifying Anticancer Drug Doxorubicin Binding to DNA Using Optical Tweezers

Zachary Ells
Bridgewater State University

Follow this and additional works at: https://vc.bridgew.edu/honors_proj

Part of the Biophysics Commons, Chemicals and Drugs Commons, Diseases Commons, Molecular Biology Commons, Nanotechnology Commons, and the Physics Commons

Quantifying Anticancer Drug Doxorubicin Binding to DNA Using Optical Tweezers

Zachary Ells

Mentor

Dr. Thayaparan Paramanathan

BRIDGEWATER
STATE UNIVERSITY
Expect More. Achieve More.

Submitted in Partial Completion of the Requirements for

Commonwealth Honors in Physics

Bridgewater State University

December 19, 2020

Quantifying Anticancer Drug Doxorubicin
Binding to DNA Using Optical Tweezers

Zachary Ells

Submitted in Partial Completion of the Requirements for

Commonwealth Honors in Physics

Bridgewater State University

December 19, 2020

_____   12/19/2020
Dr. Thayaparan Paramanathan, Thesis Advisor   Date

Edward F. Deveney
Edward F. Deveney (Dec 20, 2020 09:13 EST)
_____   12/19/2020
Dr. Edward F. Deveney, Committee Member   Date

_____   12/19/2020
Dr. Kenneth Adams, Committee Member   Date

Table of Contents

Acknowledgements

Fall 2016 I was sitting in my first ever college physics class, Physics 243 – Calculus based taught by a professor whose name was so long I could not even pronounce. Luckily, Dr. Thayaparan Paramanathan was shorted to Dr. Thaya. He saw something in me that no other science faculty saw in me before, what he jokes about now, a sport like mentality in an academic setting. From the moment he described his lab and his research I knew I wanted to be a part of it, and from there the rest is all history but a wonderful memory. Dr. Thaya proved not only to be a faculty member to me, but a mentor, life-teacher, and friend.

Dr. Thaya, first and foremost deserves recognition for everything that he has done for me, the Single Molecule Biophysics Lab (SMBL), the physics department, and the rest of the population at Bridgewater State University (BSU). He is the most thoughtful, and charismatic person I have ever met. Dr. Thaya, I want to thank you from the bottom of my heart for teaching me, not only lessons in regard to academics but also life lessons. You helped me achieve things that I was not even aware I was capable of. Although I may have hated the meetings that ran to 11:00PM, that is when I knew you were helping me the most, creating proper nuances that would last a lifetime. How to create shapes on PowerPoint that make figures, how to write my CV with proper terminology, and again the list continues. I am tremendously fortunate to have you mentor, and everything that I have accomplished in the last four years at BSU can be traced back to you in some way. Thank yous and writing an acknowledgement for you does not do you enough justice in what you have done for me!

Brian Dolle, my lab partner for the first half of the project was not only a friend but a motivator. You were always about to teach me something, whether some integration trick or how to just have a stress-free interesting conversation. I am most fond of our memory of when we were on the verge of

quitting during our first summer after eight weeks of no experimentation, to the ninth week when we were the first students to get results in the SMBL. We have shared so many moments that have kept me sane in the lab and just overall made my day.

Adam "Jabah" Jabak, where to start. You are the most genuine, nice kid that I have ever met. You always put yourself second and make sure you take care of the people you like first. Jabah I will never forget our time traveling to Peru together, our Chatta Box lunches, or our Middle-eastern talks. You always knew how to brighten my day.

I would like to thank every other SMB lab member, both past and present. Thank you, guys for having a vision, determination, and acting selflessly. Without you this lab would not be where it is today nor where it is going in the future. Us students is what makes this group so special. Thank you.

When I walked into the Dana Mohler-Faria Building of Science and Mathematics the first person I met was Dr. Edward Deveney (Dr. D). He immediately welcomed me with open arms and as we joke about was the key to recruiting me to BSU with a simple demonstration in his lab, the floating ping-pong ball. Dr. D continuously served as a role model for me, teaching me not only about physics but also life lessons. Thank you for taking your time to read my thesis and provide constructive feedback as a thesis reading committee member. The rest of the physics faculty deserve to be recognized as well for this diligent teaching. You all made me feel safe, welcome, and of course challenged. It was great few years at BSU that I will never forget because of all entirety of the department. Patty Benson gets a special shoutout for putting up with all of ordering I did. Without her my research nor any of the other research in the physics department would be possible.

Dr. Ken Adams, thank you for your guidance, knowledge, and support with the honors thesis. Thank you for taking time to make suggestions, and provide feedback making this thesis better. I appreciate all that you have done for me both inside the classroom and out.

It would improper to disregard the work that the Office of Undergraduate Research and the Honors program did for me. Dr. Shanahan deserves recognition for all of her selfless support through my time BSU. Casey O'Donnell for all of your behind the scenes support.

Amy Couto and Dr. Alexandra Adams, thank you for your assistance in writing personal statements that got me accepted to conferences and win grants that helped fund my project.

I would like to thank Dr. Mark C. Williams of Northeastern University for his support and acceptance into working his lab. Thank you to all the other lab members that are part of William's Lab, especially Dr. Michael Morse and Dr. Micah McCauley for their guidance and assistance in helping me conduct experiments. Without them the amount of data I was able to collect would not have been possible. Thank you, Dr. Ioulia Rouzina of Ohio State University, for your thought-provoking ideas and experimental suggestions in order to form a complete story.

Rob Monteith, thank you teaching me about proper milling, and for supplying the lab with flow-cell spaces at a moments notice.
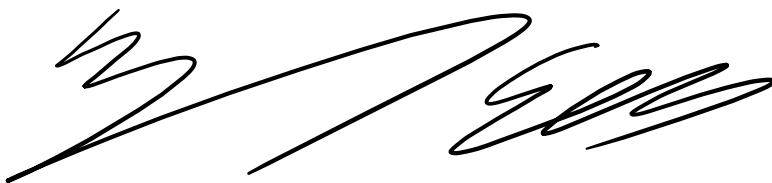
To President Clark, Provost Dr. Karim Ismaili, Board of Trustees, Dr. Kristen Porter-Utley thank you for believing in the students at BSU and pushing to enhance this school to the next level. Thank you for bringing in distinguished guests and leading companies to provide students with the opportunity for success. Dr. Ismaili thank you for a memorable summer 2018 when you would constantly visit the lab to check in on our World Cup Bracket to see who was winning. I cannot thank you all enough for your work.

None of my research would have been possible without the help of the Adrian Tinsley Summer Grant created by Dr. Adrian Tinsley who had a vision to provide students with the opportunity to conduct research on campus. I thank her for allowing myself along with countless past and present BSU students achieve academic and career goals that were out of my wildest dreams only five years ago.

To Kathy, Andy, Lexi, and Julia thank you for the endless support. Even on my most down days you all always knew how to attempt to put a smile on my face, whether with food, drinks, or something else. Thank you for baring with me as I said "five more minutes" and continued to work for another hour or two to make sure I finished. Thank you for the constant support and encouragement, where without you I surely would not have accomplished what I did over the years.

I thank the BSU community as a whole for providing a campus that always made me feel welcome, safe, and respected in every sense. To whom I did not mention directly, maintainers and chefs, I thank you as well for this would not have been possible without you, even if it was just a small chat in the dining hall about soccer or current events.

Thank you.

Zachary Ells

Abstract

As a chemotherapeutic agent heavily used since 1969, Doxorubicin's (Doxo) mission is well known and carried out, in a variety of cancers. Doxo halts cancerous cell replication and causes cancerous cells to die through inducing cellular apoptosis. The necessary concentration for this to happen and the way in which these interactions are carried out at molecular level is still under debate. We use a dual beam optical tweezers to trap and isolate a single DNA molecule so that we can explore the binding of Doxo at the single molecule level. Stretching the DNA molecule in the presence of various concentrations of Doxo allow us to quantify the binding and better understand this complex interaction. Traditional stretch and release experiments in the presence of Doxo displayed that Doxo binding was not in equilibrium. To obtain the equilibrium binding properties, the DNA was stretched and held at a constant force, allowing the drug ample time to bind to the DNA. The equilibrium extensions of DNA upon binding to various concentrations of Doxo was obtained at four different constant forces. One dimensional lattice binding model, McGhee - von Hippel Model, was used obtain the binding affinity at each force and extrapolated to obtain the binding affinity in the absence of force, K_d (0) = 1087 ± 187 nM. This very first characterization of Doxo binding to DNA at the single molecule level also yields the extension of the DNA upon a single intercalation event, Δx_{eq} = 0.40 ± 0.02 nm. The time scale of in which Doxo reaches binding equilibrium with DNA and the extension obtained upon single binding event challenges the well believed notion that Doxo is a simple classical intercalator. Understanding the binding mechanisms of Doxo to DNA at the single molecule level plays a key role to design new and improved cancer drugs for the future.

Introduction

The Red Devil

The Red Devil[1], alternatively called Red Death[2] are nicknames for anticancer drug, Doxorubicin (Doxo) due to the horrifically brutal side effects it causes to some of the patients already suffering from cancer[1]. Doxo was extracted from a bacterium species named *Streptomyces peucetius* in 1969 and introduced under the name of Adriyamicin[3], one of the first two anthracycline cancer drugs[4]. Doxo is typically used on cancer patients experiencing boundless cancer progression, and in most cases Doxo is directly injected into patient's veins to treat multiple types of cancers including lymphoma, leukemia, and breast cancer[5] to name only a few. If the dosage is not absolutely perfect then it can cause the patient to suffer cardiotoxic related side effects, where it can further escalate into death[6].

Since the introduction of Doxo in 1969 it has become one of the most used drugs worldwide as a treatment for cancers with many trade names Adriyamicin®, and Rubex®. Unfortunately, the binding mechanism of Doxo at molecular level with the DNA is still not clearly understood. Understanding this interaction is important because cancer occurs due to the rapid replication of cells, forming what is called a tumor and this process is controlled by DNA. Through the next few sections of the introduction I will graze over what exactly cancer is, how it is controlled by DNA, along with the fundament components of DNA, followed by the way in which Doxo inserts itself into the picture as a therapeutic agent.

What Exactly is Cancer?

Cancer. The dreaded word that tears families apart; a word that is ultimately recognized as being a death sentence. Cancer is not only a problem in the United States but across the world. Highlighting the United States in particular, as of 2019 it was found that cancer was the second leading cause of death in the country, second only to heart disease[7].

Every living organism is made up by cells and these cells divide and multiply to generate more cells. This is a crucial part of life as it allows for growth and the replacement of dead cells. Cancer is defined broadly as a disease caused by an uncontrollable division of cells in some part of the body.

The question that many ask; "Is it possible for a cure?" In many cases cancer can be a treatable disease with the key being early detection. There are four possible ways to combat this abnormal cell growth: (1) doctors surgically remove the mass (2) radiation therapy (3) the body attacks the cancerous cells naturally (4) chemotherapy or another type of medication[8].

The human body is wonderfully adapted to naturally combat antagonistic cells through the use of the immune system. Some cancerous cells though can evade the immune system and its ultimate destruction to proliferate further. When the cells multiply in an uncontrollable fashion, they will begin to clump up to form the well-known term, tumor. A tumor is not only found in the breasts, but also the lungs, brain, and many other parts on the body.

One may ask: well, why do cells divide and multiply uncontrollably in the first place? Now this question opens pandoras box. When a cell becomes cancerous it can happen through a variety

of mechanisms: missing/or altered proteins, DNA replication errors, environmental factors and so much more[9].

One way to stop the constant reproduction of the cancerous cell is to target the DNA, which can be done using chemotherapeutic agents, such as Doxo. To understand how this is done we must first discuss DNA and cell reproduction, which will be addressed in the next two subsections.

DNA (The Genetic Alphabet)

Since Darwin proposed the theory of evolution in 1859, DNA and proteins were debated as the genetic material of cells until 1944 when Oswald Avery proved that indeed DNA was the genetic material (The interesting history of the back and forth debate during this period is highlighted in appendix 1).The only fact that was known about DNA structure at that time was that the DNA was composed of four bases; adenine (A), cytosine (C), guanine (G), thymine (T) whose chemical structures can be seen in Figure 1[10].
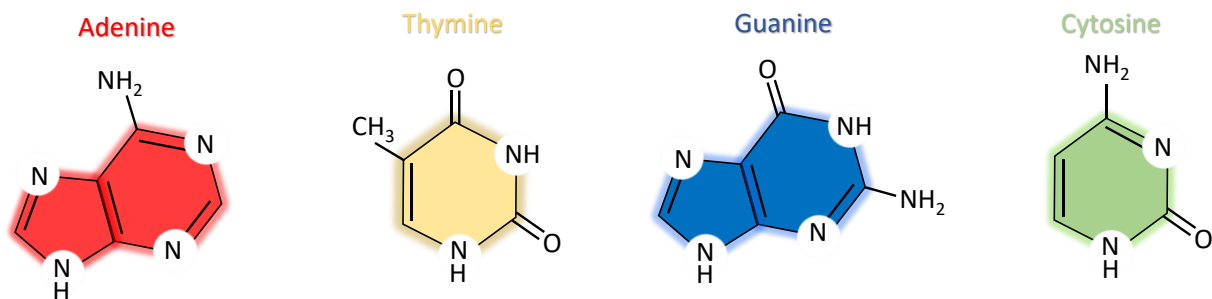

Figure 1: Cartoons representing chemical structures of the four nucleotide bases in DNA.

Erwin Chargaff in 1951 compared the amount of the four base pairs in samples of DNA from different organisms. Chargaff would conclude that each organism had the same amount of adenine (A) as thymine (T) and the same amount of guanine (G) as cytosine (C) in their DNA[11].

This discovery is vital today and known as Chargaff's Rules which led to the concept of somehow adenine pairs up with thymine and guanine with cytosine to form the DNA structure.

It was not until 1953 when Rosalind Franklin and Maurice Wilkins produced the x-ray crystallography image[12] that James Watson and Francis Crick used to determine that DNA forms a double helix structure[13]. In this structure the long chain of DNA was produced by nucleotides linked together through the phosphates; this sugar-phosphate generally referred to as the "backbone" is shown in Figure 2. The phosphate end is labeled as 5' end, and sugar end is labeled as 3' end.
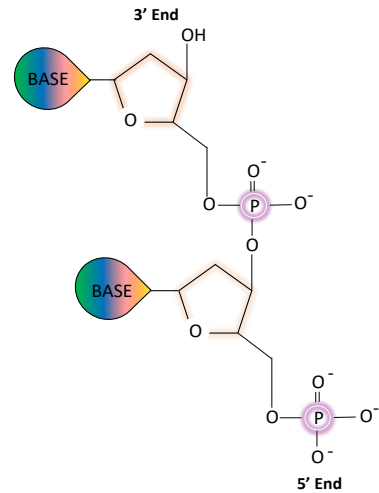
Figure 2: A cartoon representation of the DNA backbone. The pentose rings (orange) of the nucleotides are bonded through covalent bonds to the phosphate groups (purple). The bases are represented by the four-colored bubble.

Combined with Chargaff's Rule, Watson and Crick discovered that adenine and thymine will pair through two hydrogen bonds while guanine and cytosine will pair through three to create the double helix structure. A diagram showing the hydrogen bonding between the two sets of bases is shown in Figure 3.
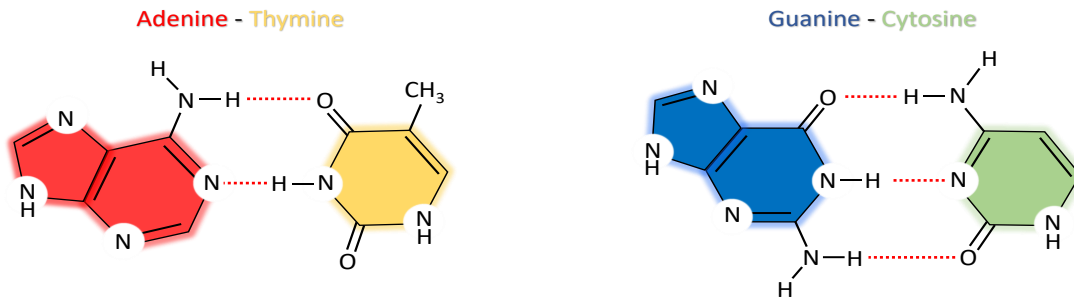
Figure 3: The electronegative atoms nitrogen, and oxygen form the two hydrogen bonds (red broken lines) between the adenine and thymine bases and the three between guanine and cytosine bases.

The double helix structure of DNA looks like a twisted ladder and is often referred to as double stranded DNA (dsDNA)[12]. The DNA gets its strength and shape as the base pairs (steps of the ladder) stack on top of each other and more pi-pi bonding interactions are created[13]. These base pairs (bp) in the DNA structure are formed 0.34 nm apart with 10 bp creating a full rotation of the double helix. The negatively charged phosphate backbone on each side of the DNA running antiparallel to each other, which can be observed through the 3' and 5' notation. This twisting of the DNA creates a groove pattern in the DNA with major and minor grooves, which alternates every 3.4 nm. A detailed representation of this can be viewed in Figure 4.
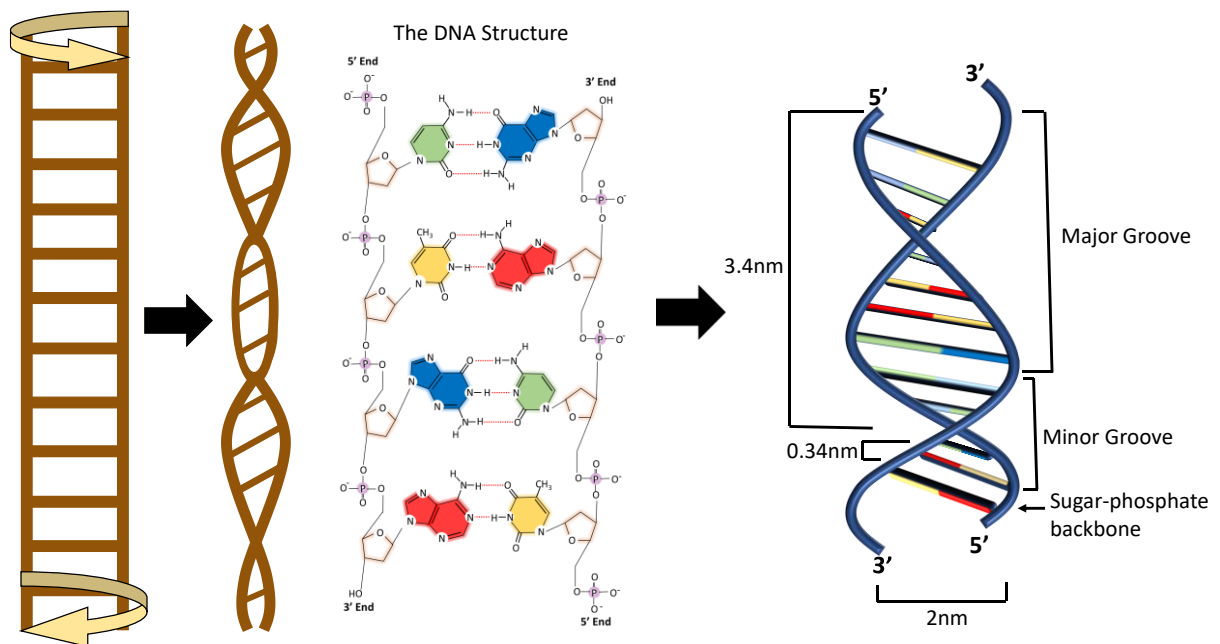
Figure 4: Simple illustration of obtaining a double helix structure by twisting a ladder (left). A detailed representation of the backbone and base pairs of the DNA in 2-dimension (middle). Schematic showing the major and minor grooves of the double helix and a full rotation of 10 bp rising 3.4 nm (right).

Cell Reproduction and DNA Replication

The human body has roughly 10 trillion cells, each containing DNA that is 2 meters (m) in length. One maybe asking themselves well how does something that is 2 meters in length fit inside a cell that is only a micron in thickness, or a tenth of the diameter of a strand of hair?

The negatively charged DNA is wrapped around a positively charged protein called a histone, which condense in groups of 8 forming what is called nucleosomes[14,15]. This complex of DNA and proteins in then referred to as chromatin. Chromatin will then be coiled into a further higher order structure called the chromosome.

All living things are composed of cells that are constantly dying and being recreated. This process is especially important for an organism to undergo growth and development. As I mentioned earlier, it becomes detrimental when a cell begins to divide uncontrollably though, and this is when it will typically be deemed cancerous. In order for a cell to function properly it requires the information that is embedded in the DNA. Therefore, when a cell divides to create two new cells the DNA has to be copied and replicated. Due to the way in which the DNA is packaged into chromosomes, it requires special enzymes to help in the unwinding process. Enzymes are a form of protein that acts as a catalyst to assist in a chemical reaction. There are two primary enzymes that help with this unwinding process, topoisomerase and helicase. These enzymes along with many other factors need to be precisely coordinated with one another during the replication of DNA each time a cell divides.

When the DNA is wrapped as tightly as it is inside the cell, it requires additional proteins to relax the supercoiling, knots, and tangles of the DNA[16]. During replication when helicase unwinds the double stranded DNA (dsDNA) and pulls it apart into two single stranded DNA (ssDNA), tension builds up in the rest of the unwound dsDNA. This creates supercoils and knots, which makes the further movement of helicase impossible. Topoisomerase binds to the twisted and knotted dsDNA region periodically to cut and splice it, so the supercoiling can be relaxed. Without this relaxing process, the DNA replication would not be possible.

This relaxation allows the helicase to continue the unwinding and separation of the dsDNA. As the helicase unwinds the dsDNA it will create what is called a replication fork (Figure 5).
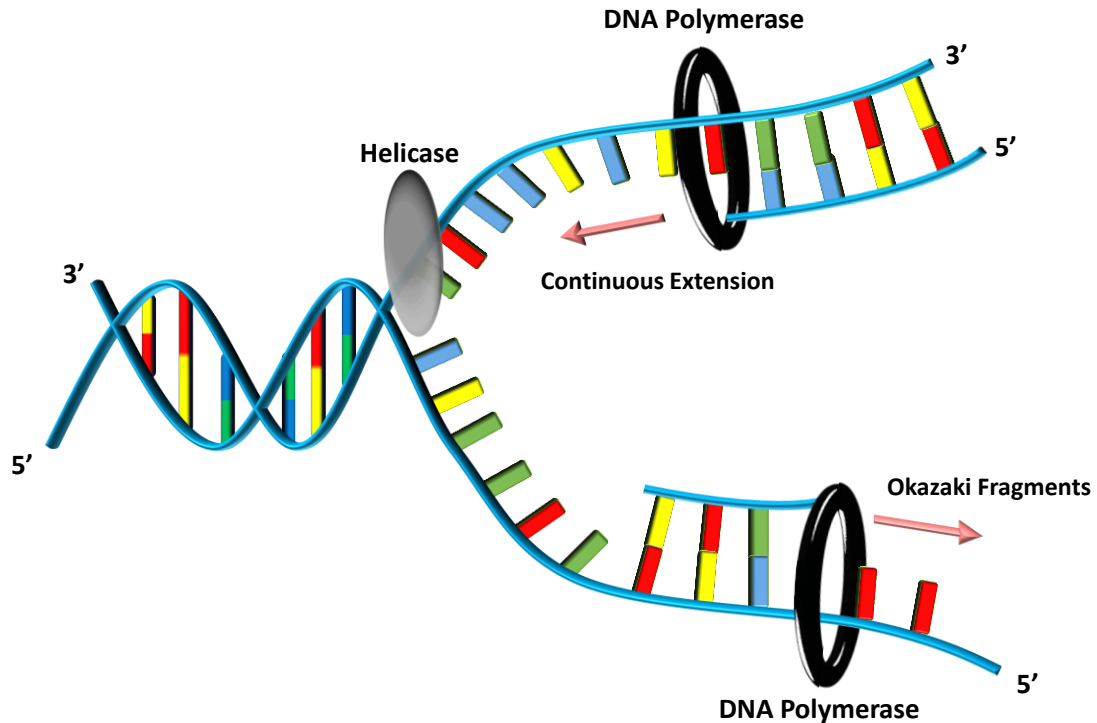
Figure 5: Cartoon depiction of a DNA replication fork where Helicase (gray) proceeds to the left to open the base pairs of the dsDNA molecule into two ssDNA. DNA polymerase (black ring) that binds to the bottom ssDNA will move towards right (from 3' to 5' direction) on the template strand and continuously place the complementary bases to form a new dsDNA molecule. But the polymerase that binds to the top ssDNA cannot move continuously as it must move towards the replication fork. Therefore, it must add complementary bases in segments that are called Okazaki fragments.

DNA polymerase (a molecular motor) will then bind the newly created ssDNA. The role of the DNA polymerase is to add the complementary base to the ssDNA creating a new dsDNA. DNA polymerase can only synthesize new DNA in one direction that is 5' to 3' on the template strand. This makes it easy for the movement along one of the strands where the complementary base will be added continuously to create the new dsDNA (top strand in Figure 5). But for the other strand the polymerase will create smaller loop fragments called Okazaki fragments, to add the

complementary bases[17] (bottom strand in Figure 5). This DNA replication process creates two dsDNA from the parental DNA which is needed as a precursor to cell division.

Fighting Cancer with Small Molecules

The molecules that have mass under 900 Daltons (a unit that is used in Physics and Chemistry to measure mass) are generally considered as small molecules[18]. These molecules can interact with DNA on the molecular level, and in some cases rapidly inhibit the replication of the cell through binding covalently and noncovalently to the DNA. Covalent binding of molecules to DNA is irreversible whereas noncovalent is reversible. Doxo falls into the category of noncovalent interactions, where if given enough time it will bind to the DNA, but it should also come off the DNA as well. Non-covalent binding falls into three major categories (Figure 6)[19] intercalation, single stranded binding, and groove binding.

Intercalation   **ssDNA Binding**   **Groove Binding**
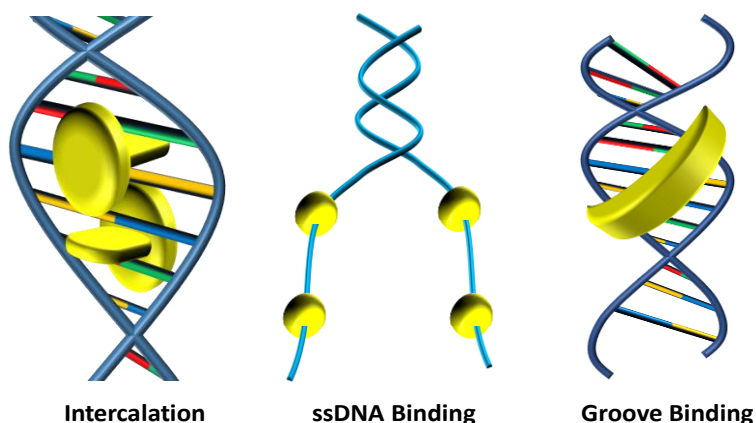
Figure 6: Different types of non-covalent interactions of small molecules with DNA. Intercalation (left) involves the sliding of a flat planer molecule between the bases of the DNA. ssDNA binding (middle) involves the interaction of the molecule with the bases when the base pairing is broken. Groove binding (right) occurs when the molecule will fit into the major or minor grooves of the DNA.

Recall the ladder analogy of DNA from earlier, intercalation is simply adding a hypothetical board between the steps of the ladder to add strength to the ladder hopefully preventing breaking. Intercalators have a particular structure where there is a flat planar section of the molecule (the

board to go in the steps of the ladder) with a bulky side piece. When an intercalator interacts with the DNA molecule it has characteristic changes where the DNA will be lengthened and strengthened. This intercalation method can act as a block to both the topoisomerase and helicase binding and preventing the replication of the DNA. Intercalators have been used for a long time as a cancer therapeutic because they act as a roadblock to DNA replication designating the cell for death.

Threading intercalators are special type of intercalators that have bulky side chains on both sides of the intercalating flat region similar to a dumbbell. To bind, these threading intercalators must thread one of their bulky side chains through the DNA bases. This extends the time for the binding and unbinding process, requiring a structural change in DNA[20-22]. Doxorubicin has been categorized as a classical intercalator where it has a flat planer section with a single bulky side chain. Typically, classical intercalators bind and unbind the DNA rapidly in the order of micro-second time scale. But you will see that our experiments show Doxo binding time scales are comparable to typical threading intercalators rather than classical intercalators.

Doxorubicin: One of The Most Prominently Used Cancer Therapeutics

As mentioned earlier Doxorubicin (Doxo) has been stamped with the nicknames of Red Devil[1] and Red Death[2] due to the distinctive hue matching that of blood, and the gruesome side effects it can cause. Despite this, Doxo and the other drugs part of the anthracycline class, including daunorubicin (Daun), epirubicin (Epi), and idarubicin (Ida), are still some of the most prominently used cancer drugs today. Up to 32% of breast cancer patients[23], 57-70% of elderly lymphoma

patients[24,25], and 50-60% of childhood cancer survivors are and were treated with the anthracycline class of drugs[26,27]. Over the last several decades, a "better anthracycline drug" has been vigorously searched for without tremendous luck.

Doxo is effective against a plethora of hematopoietic cells (immature cells that can develop into the different types of blood cells) and solid tumors, including leukemia, breast cancer, soft tissue sarcomas, childhood, sold tumors, lymphoma, along with several others[28] with an exception being that colon cancer does not respond to Doxo[29]. Regardless of Doxo's presence of being a cornerstone in anticancer therapeutics there is much more to be understood.

To halt cancer, it is necessary to cause the cell to undergo apoptosis (killing itself), and this is exactly what Doxo can trigger. The manner in which Doxo inhibits cancerous cell reproduction is the interaction between Doxo and DNA along with topoisomerase inhibition. Doxo, like other anthracyclines is known to intercalate, in which the drug molecule will have a bulky side part outside the DNA double helix while its flat-planar aromatic ring system is slid between the base pairs[30] of the DNA. This in turn increases the stacking forces within the DNA base pairs through

electron transfer, holding Doxo in place once intercalated[31]. The structures of Doxorubicin and

Doxo intercalated between DNA base pairs of DNA can be seen in Figure 7 [32].
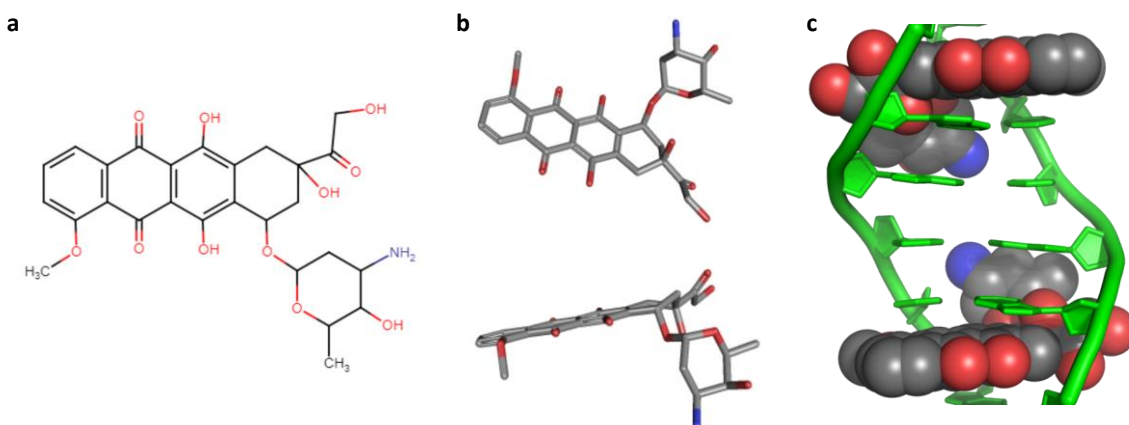
Figure 7: (a) Chemical structure of Doxorubicin (b) two orientations of 3D structure of Doxorubicin showing the flat planer section and bulky side chain more clear and (c) two Doxorubicin molecules bound to DNA through intercalation (PDB: 1D12)

This same process inhibits the enzyme topoisomerase II [33], which limits the rotational force of

the DNA during the replication process[34].

The intercalation process is left largely mystified because while Doxo intercalates it also

aggregates with itself forming dimers before and while intercalating[35-37]. This adds a level of

complexity in understanding the exact mechanisms in which Doxo interacts with DNA. Further

complicating the interaction it was reported that aside from intercalating, Doxo (positively

charged in solution) also binds to the major and minor grooves of the DNA[31]. Furthermore it has

been reported in some cases that Doxo exhibits preferential binding to particular base pairs of

the DNA. [33]

The Red Devil can rear its head in multiple ways, including cytotoxic side effects, therapy-related malignancies, infertility, cardiac, and bleeding through the palms of the hand and soles of the feet respectively from palmoplantar disease[38]. All these negative side effects limit the clinical application of the Doxo administration[39].

The detailed binding characteristics of Doxo to DNA has been reported differently throughout several published articles, causing intense debate[40]. In the millimolar range Doxo will aggregate with itself prior to interacting with the DNA[41]. In some cases reporting that it forms a dimer[36], and in others it is reported as self-association of 3 to 4 molecules of Doxo[35]. In either sense this would alter the reports of the behavior in Doxo and explains the intense debate.

It has also been reported that Doxo first binds to the minor groove of the DNA, then intercalates itself between the base pairs[40]. The only single molecule study, in which Doxo is explored is at low forces (under 10pN), its affinity to DNA is reported as $5.3 \pm 0.3 \times 10^5$ M^{-1}, and a binding site size of 1.4 ± 0.4 [35]. In other studies, binding affinity values reported for Doxo binding to the DNA ranges from nanomolar (2.3×10^8 M^{-1}) to micromolar (9.3×10^5 M^{-1})[36].

For a drug that has been used on countless patients since the 1960s there is much left to be understood regarding the interaction with DNA. In this study we quantify both the binding affinity and binding kinetics of Doxo to DNA at the single molecule level. To our knowledge only one previous study has been reported at the single molecule level and was done only at low force range using optical tweezers. We use dual-beam optical tweezers which allow us to reach high forces past the melting transition of the DNA and the ability to provide complete characterization of the drug at the single molecule level for the first time.

Introduction to Optical Tweezers

In 2018 the Nobel Prize was awarded to Dr. Arthur Ashkin for the optical tweezers and its applications to biological systems[42]. Dr. Ashkin along with Dr. Steven Chu pioneered the creation of the optical trap more than thirty years ago. Figure 8 shows what the first optical tweezer looked like that Dr. Ashkin and Dr. Chu were working with, notice the abundance of wires and
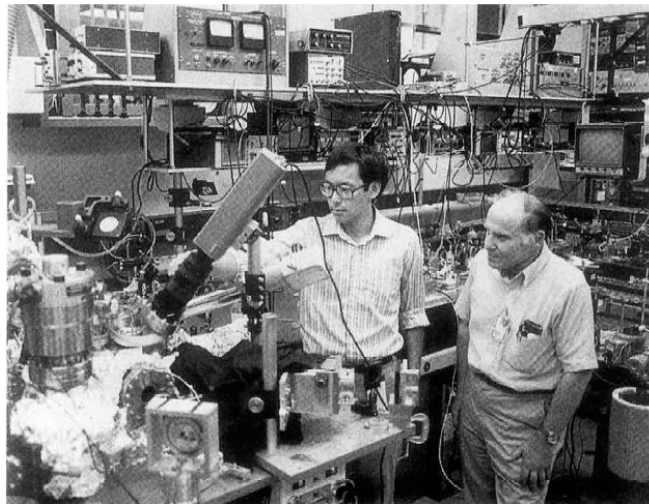
Figure 8: Dr. Ashkin (right) working with Dr. Chu (left) in 1986 at Bell Laboratory in New Jersey, USA, to trap and cool atoms using lasers.

additional equipment. In the early seventies, Dr. Ashkin published the theory to use the radiation pressure of light, to trap and manipulate small particles that would be invisible to the naked eye[43]. The theory came to fruition in 1986 when Dr. Chu was able to capture and cool atoms[44,45], which won him the 1997 Nobel Prize in physics for this accomplishment along two other scientists, William Phillips and Claude Cohen-Tannoudji. One year after the trapping of atom, Dr. Ashkin was able to trap a single virus and bacterium without damaging it in 1987[44]. The trapping of biological materials with lasers have been a challenge because water absorbs the energy from the radiation, heating up, and ultimately killing the sample. Dr. Ashkin overcame this challenge by using lasers with infrared wavelengths, where the water absorption is at the minimum. In the years to come, Dr. Ashkin was able to manipulate single cells[46], then organelles[47]. He even

reported force measurements using the optical tweezers by moving organelles within the cell[48]. This opened up a new method to study biological systems at the single molecule level.

In 2014, at BSU a president for optical trapping was set by Dr. Deveney and his students by using lasers to trap tiny (5 μm) polystyrene beads. Several years later in 2016, undergraduate students with the guidance from Dr. Thaya constructed a dual-beam optical tweezers set-up that can be used to conduct single molecule biophysics research. It is believed that this is the first set-up of this caliber that is constructed and maintained completely by undergraduate students in the Nation. There are roughly thirty of these set-ups across the world that are constructed in a similar way.

Understanding the Physics of the Optical Trapping

To understand the physics of trapping with light we first need to understand force created by momentum change during two main phenomena of light, reflection and refraction.

Imagine an introductory physics problem where there is a truck driving down a road and slams into a tree, bouncing off. Now think about the light from a simple laser pointer being pointed off a mirror and reflected in a different direction. What is the similarity between the two events? In both events the truck and light carry a linear momentum which caused them to bounce off an object. It is easy to understand that a truck carries linear momentum (mass × velocity), but it is more complex to imagine that light can also have momentum. This can be explained by combining quantum mechanics and wave-particle dual nature of light.

With that said, Newton gave the equation of $F = \frac{dp}{dt}$, meaning that there is force that is represented by the rate of change in momentum. In the previous example the rate of change in momentum of a truck is much greater than that of a laser, therefore the force associated with the laser is minute. Although we, as humans, may not necessarily feel a force from a photon there is a force and pressure applied to a particular location of impact The pressure created by the force is proportional to the force: $P = \frac{F}{A}$, where F is force, P is pressure, and A is area. Substituting for force from Newton's Law mentioned above you get: $P = \frac{1}{A}\frac{dp}{dt}$. This equation is saying that there is a particular pressure associated with the laser reflecting off a mirror, this is deemed the radiation pressure.

Just like the reflection of light can cause change in momentum and in turn result in a force as discussed above, another phenomenon of light known as refraction can also result in a momentum change and lead to the creation of force. The speed of light changes depending upon the medium in which it is propagating through. When light transitions from one medium to another it will bend, and this is bending of light known as refraction.

Snell's law describes the bending of light at the interface of the two mediums, which states that $n_1 sin\vartheta_1 = n_2 sin\vartheta_2$, where n_1 and n_2 are refractive index of the mediums. Mediums are given refractive indexes based on the speed of light in that medium. The angles ϑ_1 and ϑ_2 are the angle made by the incident beam and refracted beam respectively with the normal.

In the case of the optical tweezers, the laser will be passing through the liquid buffer medium (with refractive index n_1) to the polystyrene bead (with refractive index n_2) as shown in figure 9. Since n_2 is greater than n_1, the incoming ray (red) will be refracted (green) towards the normal according to Snell's law as shown in Figure 9. Some of the laser radiation will also be reflected (brown).

On the way out of the bead it will bend away from the normal. The refraction of two symmetric laser rays passing through a bead in the center of the laser beam is shown in Figure 10.
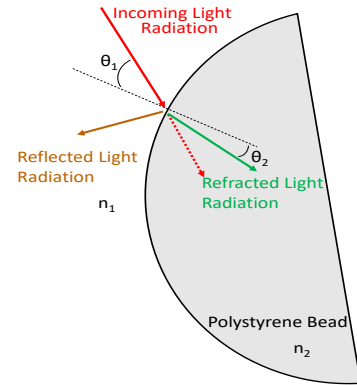
Figure 9: Application of Snell's Law as it pertains to the optical tweezers. Incoming laser radiation (red) from the buffer medium, makes impact with the surface of the bead where part of it is reflected (brown) and the rest is refracted (green).
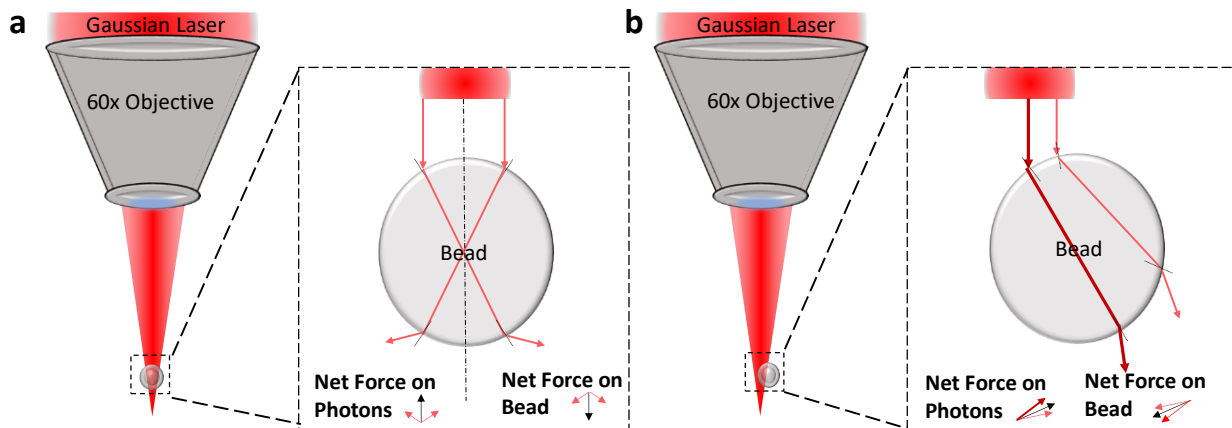
Figure 10: Schematics of a laser focused by an objective onto a single micron sized point holding a bead in place and Ray diagrams explaining the physics. (a) The case where the bead is along the optical axis of the objective and the enlarged view describing the symmetric rays refracting through the bead. The left inset shows the momentum changes of both beams (light red arrows) resulting in the net force (black arrow) on photons. The right inset shows the equal and opposite force acting on the bead. (b)The case where the bead is entering the laser beam from the left and the enlarged view describes an intense ray from the center of the laser bean and less intense ray from the edge of the beam getting refracted through the bead. The insets describe the forces on the photons and bead.

The bending of light while passing through the bead creates the momentum change of the photon, and henceforth a force of the photon. From this we can figure out the direction of the net force acting on the bead which will be opposite of that on the photon. The resulting force in the symmetric case will be in the direction towards the focal point of the objective (Figure 10, left). When the bead is misaligned and away from the axis of the laser (Figure 10, right), the gaussian nature of the laser will still trap the bead. That is because the middle part of the laser emits more intense radiation, therefore it will apply more force on the bead pushing it towards the center optical axis.

Trapping and Stretching DNA with Optical Tweezers

When the bead that is trapped is pulled out of the trap by a force the laser gets deflected and that deflection can be measured using detectors and then converted to force measurements. This concept is used to tag biological molecules to the bead to obtain force measurements. Dr. Steven Block was able to trap a single DNA molecule and stretch with optical tweezers and measure the force experienced by the DNA as function of extension in 1997 [49]. This results in the force-extension curve commonly known as DNA stretching curve (Figure 11). You can see that the forces experienced while stretching is in the order of pico-newton (pN), which is 10^{-12} N and is very small and comparable to the forces exerted inside the living cell. This makes optical tweezers a great tool to study the force responses of biological materials.
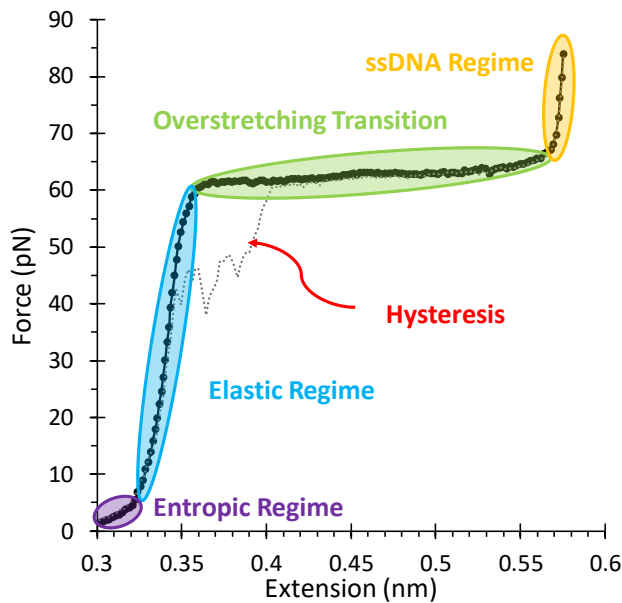
Figure 11: DNA stretch (black circles – black solid line) and release (black dashed line) curve with the four important regions highlighted. Entropic Regime (purple), Elastic Regime (blue), overstretching transition (green), and ssDNA (yellow). When enough time is not given the DNA may not properly reanneal resulting in hysteresis while the release (red)

DNA stretching is a reversible process where when it stretched and then given ample time to return it should return exactly the way it began. The black line in Figure 11 represent the force measured while stretching the DNA and the black broken line represents the release of the DNA.

At the beginning of the stretching in the bottom left highlighted in light purple in Figure 11 the DNA is slack with all the base pairs properly annealed. Not much force is needed to stretch it to its natural length to make it taut. When we make the DNA taut, we are reducing its entropy therefore this region is referred to as the entropic regime. Once the DNA is taut further pulling makes the backbone of the DNA respond by beginning to untwist. This phase of DNA stretching can be modeled similar to that of elastic band, or spring, where the DNA is fighting to be

stretched[50]. This second region highlighted blue in Figure 11 is known as the elastic regime. In the elastic regime there is little extension seen but a large increase in force response from DNA which increases from near zero to 65 pN. After reaching 65 pN you can see that the DNA length is almost doubled without much change in the force. This region shaded green in Figure 11 is labeled as the overstretching transition. There have been multiple models that has been debated over the year on what's happening to the DNA in this region[51,52]. After almost twenty years have passed since the first DNA stretch, now many agree that the DNA base pairs begin to break and that causes the greater extension of the DNA without much of an increase from the 65 pN force. This is referred to as Force Induced Melting (FIM). The DNA goes through a phase transition from dsDNA to mostly ssDNA at constant force, similar to ice melting into water at constant temperature. The last regime (highlighted light orange in Figure 11) is the ssDNA regime where most of the bases of the DNA are broken except regions of the DNA that are GC rich. Upon release of the DNA from the ssDNA regime the bases begin to reanneal. Occasionally the DNA will not properly anneal resulting in the hysteresis seen in Figure 11 indicated by the red arrow. Figure 12 depicts a cartoon describing the state of the DNA in each regime of the DNA stretching curve.
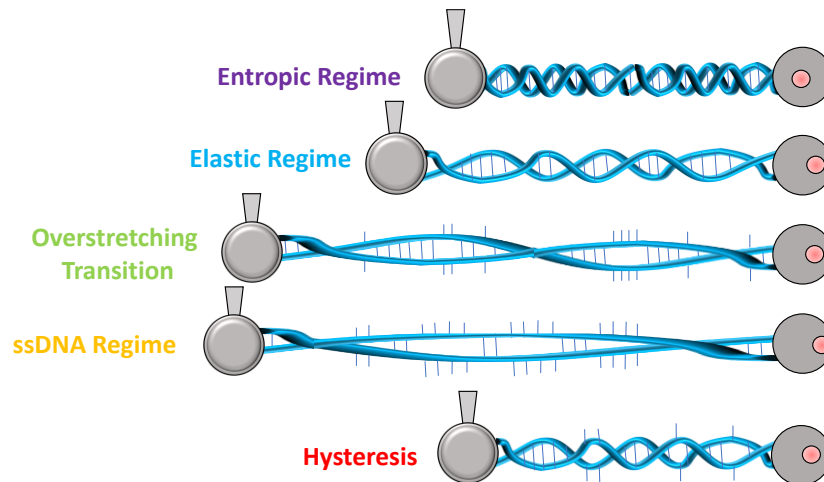
Figure 12: A cartoon representation of what the DNA could look like in each regime of the DNA stretching process. In entropic regime DNA is in its natural state, bundled and slack. In the elastic regime the DNA begins acting like a spring resisting stretching. Overstretching transition, the base pairs begin the melt except for regions that are rich in GC content. In the ssDNA regime most of the base pairs are broken apart. Upon the relaxation the DNA begins to reanneal back to its original form, sometimes not matching up perfectly though resulting in hysteresis.

Studying Intercalation using the Optical Tweezers

Understanding how the DNA stretching curve changes when the DNA is stretched in the presence of an intercalator provides insight into the binding mechanisms and strength of binding. Models hence have been developed which quantify these interactions between the DNA and these molecules[53]. Obviously when intercalators insert their flat parts between the DNA base pairs, the DNA will have a corresponding lengthening. This DNA lengthening can be seen in the DNA stretching curves as indicated by the blue arrows in Figure 13.
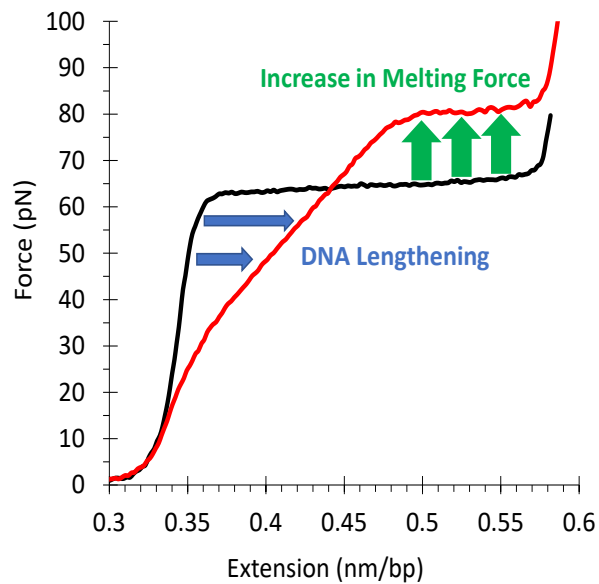
Figure 13: DNA stretching curve in the absence (black) and in the presence of an intercalator (red). Highlighting the associated increase in length (blue arrows) and increase in force required to melt the DNA (green arrows) in the presence of intercalator.

Imagine you have two glass sheets stacked on top of each other, it is relatively easy to pull the two apart from one another. Now, add water, that task becomes a lot more difficult than the previous attempt. The premise is the same with an intercalator when it is added to DNA. Initially it is easy to pull the DNA apart but when an intercalator is added the task gets more difficult.

As the intercalator inserts itself into the DNA it is increasing the pi-pi bonding between the base pairs strengthening the DNA. In experiments this is seen through needing an increase in the force needed to melt the DNA during the overstretching region (Figure 13)[18].

Both of these effects, the lengthening of the DNA and increase in the melting force, increases as we add more intercalators. This is clearly visible in Figure 14 [54] where DNA is stretched in the presence of various concentrations of a classical intercalator EtBr. You can also observe that after

certain a critical concentration (125 nm in this example) the melting transition disappears

indicating the impossible nature of melting the dsDNA in the presence of intercalator.

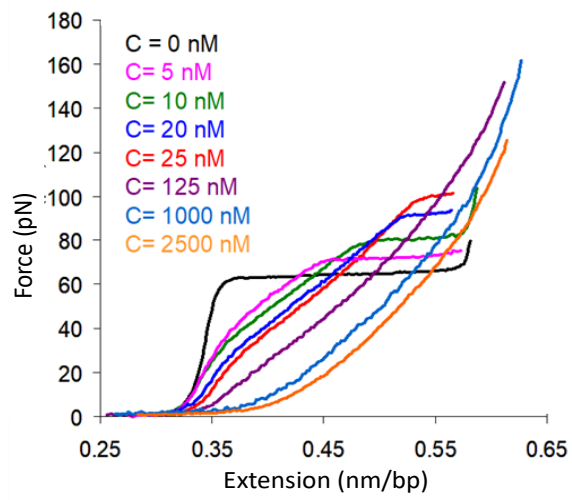*Figure 14: DNA stretching in the presence of various concentrations of a well-known classical intercalator, Ethidium Bromide (colored curves) and in the absence of the intercalator (black).*

Materials and Methods

Preparation of Biomaterials

In our experiments we use four main biomaterials: buffer solution, polystyrene beads, DNA, and the drug under investigation (in our case Doxo). All of which requires the buffer solution for preparation. Our buffer imitates that of the physiological conditions seen inside the body, which has a pH of 7.4 and a salt concentration of around 150 mM. The buffer solution we prepare is done so by combining 5.885 g of NaCl, with 10 ml of 10 mM Tris, and 990 ml of Milli-Q water (special water that has gone through a series of deionization and filtration steps to maintain a resistivity of 18.2 MΩ cm). The buffer is then filtered and tested to have a pH of 8, slightly more basic than physiological conditions along with a salt concentration of 100 mM which is slightly lower than the physiological condition.

The biosafe beads that we use in our experiments are bought from Spherotech. They are 3.11 μm diameter polystyrene beads that are coated with streptavidin (SVP-30-5).

The lambda phage DNA (48,500 bp) used in our experiments are purchased from Sigma-Aldrich and labeled with biotin on the 5' ends in the lab. This labeling enables the tethering of DNA to the beads by forming streptavidin-biotin complex (Figure 15) when introduced into the system.

Streptavidin **Biotin** **Streptavidin – Biotin Complex**
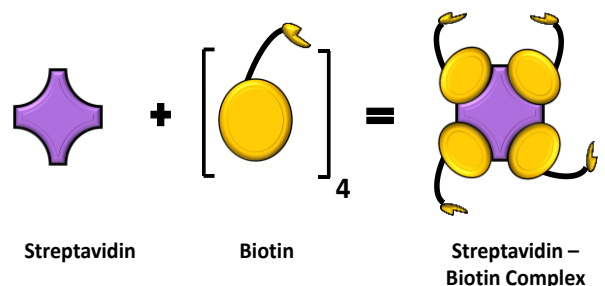
Figure 15: Cartoon showing the binding mechanism of streptavidin and biotin that allows the biotin labeled DNA in our experiments to chemically attach with streptavidin coated beads.

Doxo was bought as a powder from Fisher Scientific (AAJ64000MA) and a stock solution of 11.49 mM was made by adding 10 ml buffer. By taking 4.35 µL from the stock and mixing with 495.65 µL a sub-stock solution of 100 µM. Before every experiment was carried out the sub-stock eppendorf tube was vortexed well to assure the solution was properly suspended. This was done because the drug could have been sitting for a long period of time in between experiment, and because we read that the drug can aggregate in the millimolar range. Although that is far away from our micromolar range we did so out of precaution. The concentration of the drug was also occasionally double checked with absorption spectroscopy. For each experiment, the exact concentration of Doxo needed was calculated by hand and then assured using a calculator built into our data analyzation program. The solution was then made in the reservoir tube and ready to be used in the experiment once mixed.

The buffer is stored in a sterile 1 L plastic container at room temperature while the rest of the biomaterials are stored in a temperature-controlled refrigerator at 4°C. Upon need of a particular biomaterial, it was removed from the refrigerator prepared, pipetted in the respective reservoir tube and then immediately placed back into the refrigerator for preservation.

Dual-beam Optical Tweezer Set-up in the Single Molecule Biophysics Lab

The SMB Lab, where the optical tweezer set-up is kept, is in a temperature-controlled room at 25°C. The entire set-up is built on an optical table that roughly weighs 800 pounds which sits on four cylinders that are supplied with air from an external compressor. This air then causes the table to rise and float allowing for the system to be isolated from vibrations in the environment.

Since the forces measured in our experiments are in the order of pico-newtons any vibrations that come from walking down the hallway, or to doors slamming in the building will have to be isolated and the optical table does this job. Any vibrations or changes in temperature will also alter the laser alignment, which is exceedingly difficult to obtain in the first place. An image of the optical tweezer set-up at BSU can be seen in Figure 16.
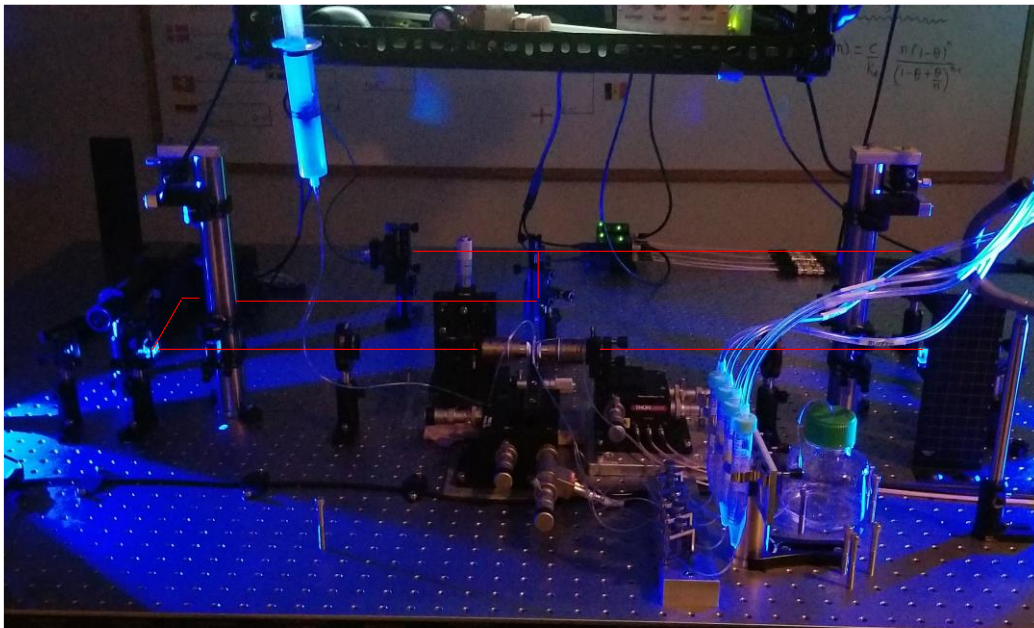
Figure 16: The dual beam optical tweezer set-up at BSU. The laser which is not actually visible is depicted here with red line to visualize the laser beam path.

In our dual-beam optical tweezer, a single beam from laser gets split up into two separate pathways and then gets finely focused onto a single micron sized point. A micron sized point is equal to one-hundredth of the thickness of a single piece of your hair. The reason for the dual-beam optical set-up opposed to a single beam apparatus allows for us to reach higher forces. Figure 17 represents a bird's eye view of the details and components involved in making the functional dual beam optical tweezers at BSU.
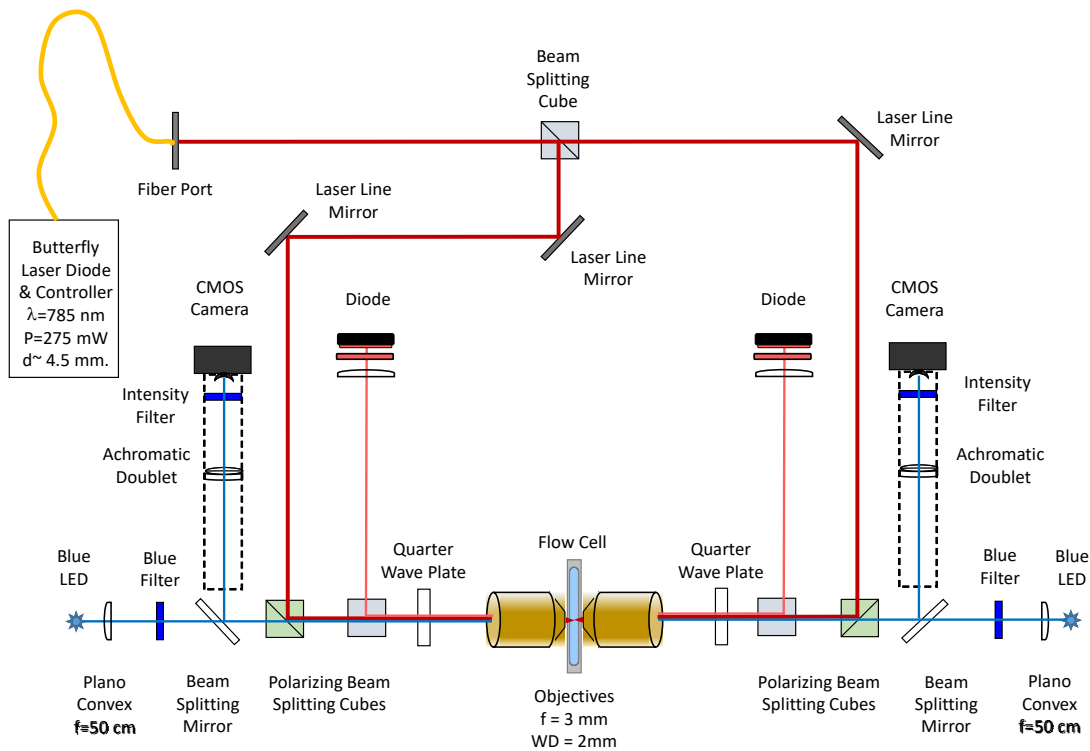
Figure 17: Schematic of the dual beam optical tweezer set-up and the components used at BSU

We use a single butterfly laser diode to produce a beam that is just out of the visible spectrum of light and in the inferred spectrum. A full component break down of the components of our table can be found in[55]. The 275 mW beam, linearly polarized to be vertical to the table exits through the fiber port, travels to the right on the diagram to the first beam splitting cube where the single beam now becomes two with equal power. Each beam then encounters a series of mirrors to reach the polarizing beam splitting cubes (shaded in green) at the bottom of Figure 18Figure 17.

Disregard the blue lines on the edges of Figure 17 for the moment and continue to follow the red laser line on the left.

The polarizing beam splitting cube is designed in a manner to split an un-polarized laser into two perpendicular linearly polarized beams. When its reflecting plane is placed at 45° to the incident

beam such that the plane is vertical (Figure 18)[55], polarized vertically, and the transmitted laser will be polarized horizontally.

In our set-up the green colored polarizing cube is used primarily to steer the vertically polarized laser in the direction of the objective through reflection. The second polarizing beam splitting cube (color coded in blue in Figure 17) is placed in an orientation such that the vertically polarized beam will be transmitted and any horizontally polarized light to be reflected directly up towards the director.

Figure 18: The beam splitting polarizing cube reflects the vertical polarization that is parallel to its reflecting plane (green) and transmits the horizontal polarization (yellow) through the cube.

Therefore, our vertically polarized beam from the left will be transmitted through the cube to reach the quarter wave plate.

The quarter wave plate will alter the polarization of the beam making it circular before entering the objective. The objective then focusses the laser inside a microfluidic flow chamber that we call the flow-cell, where we trap the beads and the DNA to conduct our experiments. The objectives used in our set-up have 60x magnification with a working distance of 2 mm and a numerical aperture of 1.2. Numeral aperture is measure of how the light is bent while focusing the laser and depends on the refractive index of the medium. Higher numerical aperture will result in a stronger trap.
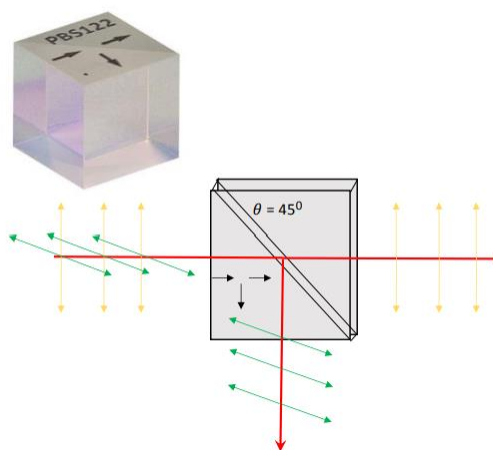
When the laser passes through the trapped polystyrene bead and emerges out from the opposite objective it will pass through the other quarter wave plate (on the right) making the laser linearly polarized again but with a 90° rotation. This means that after the laser passes through both quarter wave plates (through the objectives) it will be horizontally polarized.

As the horizontally polarized laser then encounters the polarizing beam splitting cube on the right side of the objective (color coded blue in Figure 17) it will be reflected towards the diode detector. A lens with a particular focal length and an intensity filter prior is used to focus the laser into the diode detector and protect the diode from high intensity. This diode detector measures the deflection of the laser and from that we can extrapolate the corresponding forces.

Now consider the blue line that represents the light that comes from the blue LED on the left side. This provide collimated light to the objectives to illuminate the flow-cell, which will be discussed shortly. This light then is directed to the opposite camera to provide the image inside the flow-cell. All the optical components discussed above will not have any effect on the blue light because of its random polarization.

An achromatic lens prior to the camera is used to focus the image and a particular bandpass filter is used exclude the unwanted light entering the camera. This unwanted light would distort and take the image impossible to see. These cameras are projected into a computer screen that allow for us to visualize and manipulate the experiment.

The laser beam and blue light travelling in the opposite direction will follow a similar path as described above for the beam travelling from left to right.

The Flow-cell

Our entire experiment is conducted in what is called a flow-cell which can be seen in Figure 19. These flow-cells are hand constructed at BSU where we get the plexiglass spacer from the machine shop with three holes drilled in it (the micropipette tip hole, waste tube hole, and a hole for the four inlet tubes) and a hollow channel in the middle. The flow-cell is then cleaned using dish soap and dried, then further cleaned using methanol. This is done rigorously to remove any oils or contaminants from the milling process.
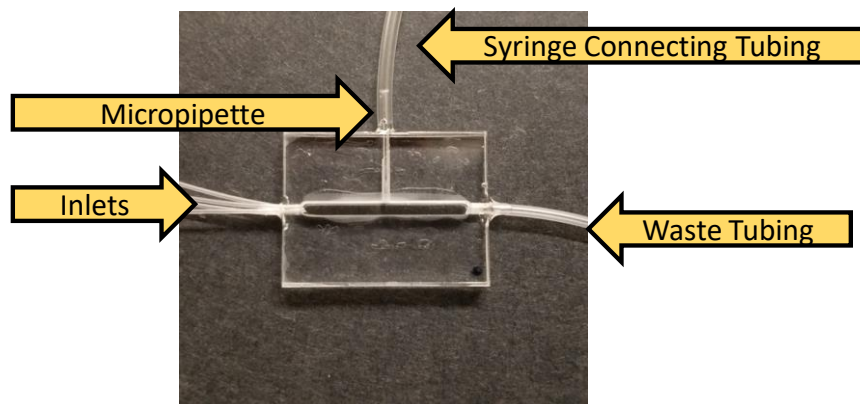
Figure 19: A hand-constructed plexiglass flow-cell with four inlet tubing (left) that allows to the flow the biomaterials, a waste tubing (right) which collects the liquid waste from the experiment and micropipette tip (top) inserted into the flow-cell through vertical channel and connected to a syringe.

An optical adhesive (NOA68, 6801, Norland Products) is added to one side of the plexiglass spacer evenly and microscope cover glass slide (22 x 30 x 0.13 mm, 12-545A, Fisher Scientific) is then placed precisely and carefully on the adhesive. Its then exposed to UV light for 45 minutes to cure the glass slide to the plexiglass spacer. This process is repeated for the other side to obtain a chamber.

A borosilicate glass micropipette tip (TIP1TW1, World Precision Instruments) is then inserted through the top vertical channel. Inserting this glass tip takes precision and requires the use of a microscope with 100x magnification to slowly move the tip down the channel hole. Any bumping of the tip on the side of the channel will cause the single micron sized tip to crack, ruining the entire flow-cell causing a restart of the process.
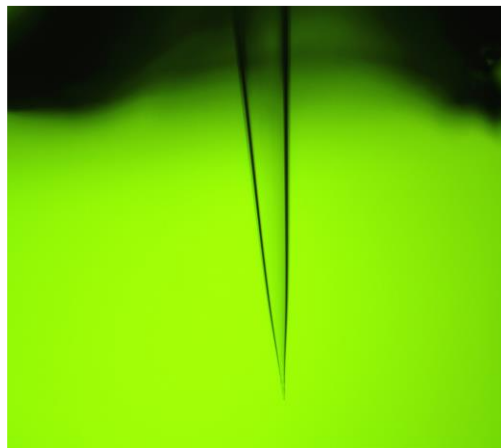
Figure 20: The micropipette tip inside the flow channel viewed under a 100x microscope.

Figure 20 shows the image of the tip under the 100x microscope. The micropipette glass tip is adjusted until it is placed directly in the center of the main flow chamber. Once perfectly placed a dab of the optical adhesive is used and exposed to the UV light for 45 more minutes to secure the tip in place.

After the curing process a diamond tipped pen is used to break the excess of the micropipette tip leaving only a single centimeter exposed. A 7-inch long piece of Tygon® Microbore tubing, with inner diameter of 0.020" and an outer diameter of 0.060" (EW-06419-01, Cole-Parmer), is used to fit directly around the micropipette end. It is then sealed with optical adhesive using the same procedure as before.

Next the four BD Intramedic Polyethylene tubing (PE10, VWR) are inserted to one of the sides of the flow-cell to be used as inlets. These four tubes are cut to be about 8 inches long and have an inner diameter of 0.011" and an outer diameter of 0.024". Once placed through the hole into the flow-cell chamber it is important to carefully maneuver the tubes to the edge of the hole not having too much of the tubing inside the chamber. Having too much tubing inside the chamber

or not aligned with the edge of the drilled hole will cause turbulent flow of the biomaterials. The optical adhesive and UV light procedure is once again carried out once the tubing is placed properly. The reason to have four inlet tubes is for the four types of biomaterials needed to carry out the experiment. Buffer, polystyrene beads, Λ-DNA, and the drug of interest that is being studied.

Finally, nearly a 12" long BD Intramedic Polyethylene tubing with a inner diameter of 0.045" and an outer diameter of 0.062" (PE 160, VWR) is inserted into the third hole of the flow-cell to serve as the outlet tube (waste tube). Similar to the four inlet tubes the waste tube needs to be places perfectly in the remaining side hole to the flow-cell chamber. Once placed, again the adhesive and UV light combination are used to seal. The flow-cell is now ready for experiments. The replacement of the flow-cell is required only when the drug in the chamber and cannot be completely washed away with buffer and a molecular cleaner, Tween, (this commonly happens at high concentrations of Doxo) or when the flow cell leaks.

Biomaterial Reservoirs and the Flow Control Process

The biomaterial reservoirs are used to feed the flow-cell the needed biomaterial through its inlets during the experiments. These reservoirs are designed with 15 ml tubes with a custom drilled hole in the bottom of them (the holes are drilled in the machine shop).

The same type of tubing that is used for the waste tube of the flow-cell is used as the outlet of the reservoirs. A 9" piece is placed inside the hole and sealed using the optical adhesive and UV light to cure. Each of the four reservoirs are then placed in a special designed biomaterial

reservoir holder to hold each one independently. This is a custom-built reservoir holder designed by SMBL lab members in 2017. Each tubing is then placed through separate clamp gates (circled in yellow in Figure 21). In addition to allow the flow the clamps are used to prevent backflow into the reservoirs when they are not in use.

The way we are able to flow the desired fluid at a particular time is due to the fact of compressed air. Each reservoir has a cap that is attached to a tubing (circled red in Figure 21) and connected to a solenoid valve. The solenoid valves are connected to the compressed air system and controlled by a custom-built electrical flow control box (built by me in 2018). With a flip of a switch from the electrical flow control box (Figure 22) it is possible to flow the desired fluid into the flow-cell. When the desired switch is flipped on the flow control box it will causes a solenoid to displace allowing air to flow through the valve into the tubing that is connected to the cap of the reservoir. This air pressure will push the biomaterial in the reservoir into the flow-cell.
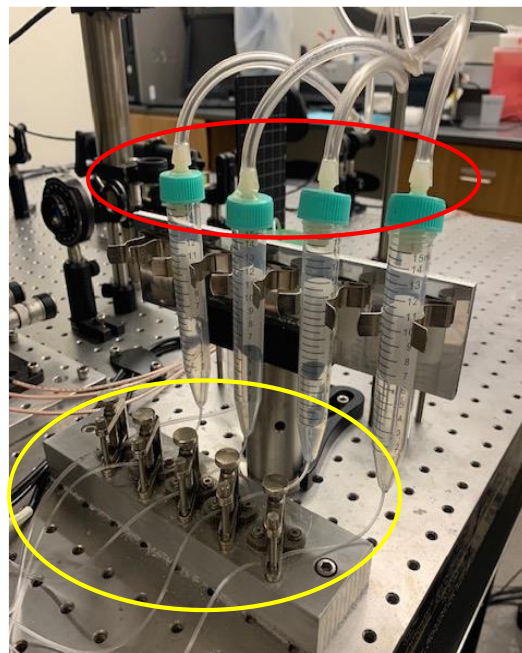
Figure 21: The clamps (circled in yellow) that serves at gate for biomaterial flow from the reservoir. The tubing attached to the caps of the reservoir tubes (circled in red) connects to compressed air flow.

Figure 22: Custom designed flow control box to flow our four biomaterials. Upon flipping of a single switch, it will induce the solenoid (not shown) to move a magnetic clamp allowing for compressed air to flow through the tubing to the reservoir holders at adjustable pressure.

Connecting the Flow-cell to the Biomaterial Reservoirs and cleaning

Once the flow-cells and the biomaterial reservoirs are completed they should be connected, and a series of tasks must be completed prior to the start of an experiment. The edges of the tubing to the four inlet tubes are trimmed diagonally to assure that we do not get any dust or other contaminants into our system. This freshly cut tubing is then connected to the tubing that comes out of the reservoir tubes as shown in Figure 23. The waste tube is connected to the waste container, and the tubing from the micropipette tip is connected to a syringe.
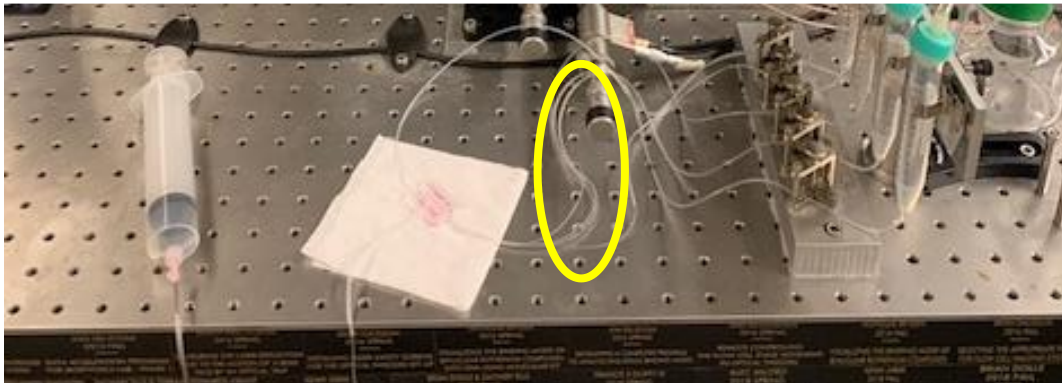
Figure 23: The flow cell inlets connected to reservoir tubing (circled in yellow), the waste tubing connected with waste connected with waste container and micropipette tubing connected with the syringe.

The new flow-cell that is attached to the biomaterial reservoir system is flushed with two milliliters of buffer from each of the four different reservoir tubes independently. This flushing with buffer accomplishes cleaning the system of any dust particles or unseen contaminants. Once the flow-cell is flushed then a little bit of buffer is added in all four reservoirs and flowed through the tubing. But this time the purpose is to fill the system with buffer such that there are no air pockets or bubbles in the system.

Are we ready for the experiment yet?

Now that the flow-cell has been properly hooked up the reservoirs, washed out and filled with buffer we are now ready to place the flow-cell between the microscopic objectives. The flow-cell is placed on a moving stage that can be manipulated by hand and piezoelectric controller. This must be accomplished using steady hands, and precision without scratching the objectives. As seen in **Error! Reference source not found.** the stage clips (yellow arrows) are separated to wedge in the flow-cell between them and the whole flow-cell is then slid down into the clamps.

The reason for such diligent work is that if the objectives are bumped or displaced the alignment of the laser will have to be redone which can take hours to up to weeks to fix. The stage (Figure 24) allows for manual movement of the stage in three dimensions along with fine nanometer movements in one direction. A piezoelectric crystal within the stage that expands or contracts with applied voltage allows for the fine movement of the stage in one direction. During experiments this is controlled by the computer program to move the stage to
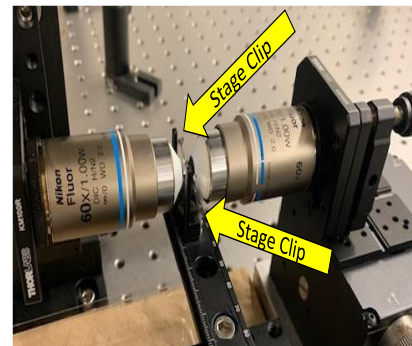

Figure 25:The flow-cell dock and clips that hold the flow cell in place mounted in the piezoelectric stage.

Figure 24: The stage (front) that is used to mount the flow-cell. The two shorter length knobs (coming towards the front and left) are for manual control and the longer knob coming towards the front can be manipulated both manually and by the computer.

stretch the DNA. Now that we have the flow-cell docked on the piezoelectric controlled stage, we are ready for the real action.

Lights, Camera, Action

Before turning on the laser we need to understand the operation conditions of the laser. The laser selected for the optical tweezers contains particular characteristics necessary for the functioning of the experimental set-up. The laser used in the BSU SMB lab is a butterfly diode laser that is housed in a compact LD and temperature controller as seen in the Figure 26. The controller is hypersensitive to electrical surge so before touching it is of up most

Figure 26: Laser controller that houses the laser that is used for the optical tweezers.

importance that the researcher grounds themselves before turning on the controller. As the laser controller boots up to the screen seen in the figure 26, the internal temperature is set to its operational temperature of 25°C. Once the temperature reaches this value, the laser warning sign at the entrance of the lab is turned on for safety, and then the laser is turned on. The laser has a power of 250 mW and a wavelength of 785 nm which is just outside the visible spectrum towards inferred. The laser transmits through all the optical elements as discussed earlier in the optical tweezers set up.

To see the image of the flow-cell while the experiment is happening, we use blue LEDs on both sides of table (as we discussed earlier, Figure 17). These blue LEDs are used to illuminate the flow-cell allowing for an image to be created in the camera. There is an adjustable setting on the blue

light that allow us for the brightness to be adjusted as needed. These cameras are connected to a computer above the optical tweezers dedicated to process the camera image. Through a program we can select which camera we would want to see on at a specific time. Throughout the experiment we shuffle back and forth from one camera to the other.

The Game Plan

The overall idea of the experiment is to trap a bead with laser and attach it to the micropipette and trap another bead to be held by the laser. After trapping the beads, DNA is flown through the flow-cell and a single DNA molecule is chemically attached between the two beads. The DNA is stretched to check if it is a good candidate for experiments. If it is good DNA the drug is added to the system and then the DNA is stretched in the presence of the drug. Figure 27 illustrates the main steps of the experiments, which will be discussed in detail in the coming sections.

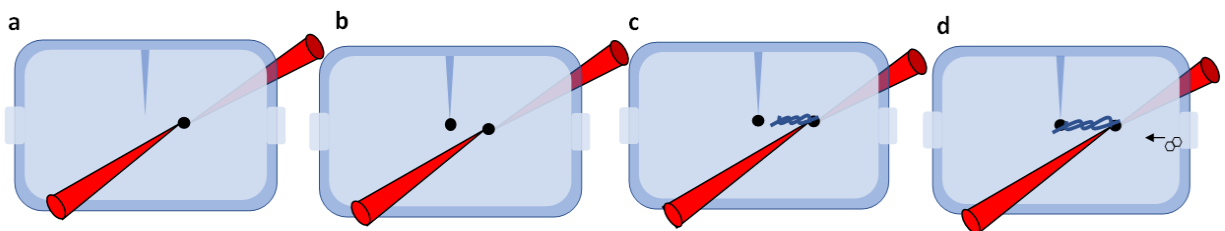*Figure 27: Process of catching a single molecule of DNA inside a flow cell with optical tweezers. (a) Polystyrene bead caught in laser trap. (b) First bead attached to micropipette tip and second bead is captured in the laser trap. (c) DNA is introduced into the system and one end is attached to the bead in the trap. (d) Other end of the DNA is attached to the bead on the micropipette tip and drug introduced into system.*

Trapping Bead and Checking the Laser Alignment: Obtaining a Stiffness Curve

The first step of our experiment is to check the strength of our trap and fine alignment. This is done by trapping a bead and obtaining a curve called stiffness curve.

The bead reservoir is filled with 2 ml of buffer and 2 µl of 3.11 µm polystyrene beads coated with streptavidin is added and vigorously mixed so that the beads are equally distributed throughout the reservoir tube. The beads flow is turned on until a bead is trapped.

The trapped bead is then attached to the micropipette tip via suction using the syringe and the rest of the system flushed of stray beads. The bead on the micropipette tip is moved across the laser spot using the computer program to obtain the trap-stiffness curve (figure 28).

In the trap-stiffness curve although the y-axis is marked "force" and the x-axis is marked "position", you will see that the units of the force is marked as microns.
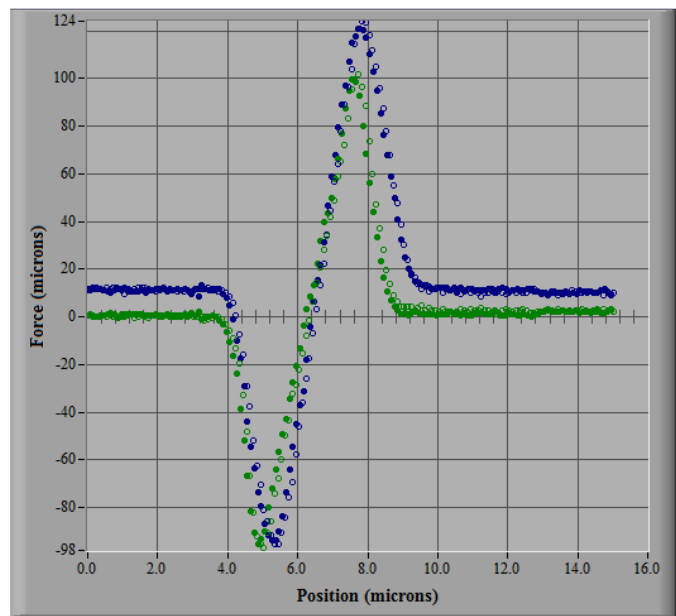
Figure 28: Screenshot of our program showing a stiffness curve obtained prior to an experiment. The blue and green dots represent the deflection of the laser as the bead passes through the laser spot by the detectors on either side.

The reason behind this is the program is essentially plotting the deflection of the laser beam due to the bead moving into the trap. The reason we see two different plots (blue and green) on the graph is because we have two diode detectors on either side (refer to Figure 17). The solid circle

represents the micropipette tip moving away from the origin initiated while the open circle represent the return. If the alignment is perfect, both plots should overlap and most importantly both curves should have the same slope. If they do not overlap, fine laser alignment is needed and carried out by adjusting the fine adjustment controls for the piezoelectric stage.

Once we have the alignment done, we move the bead attached to the pipette away from the laser spot and trap another bead with the laser. The system is then flushed of the stray beads with the buffer. Now we have two beads one attached to the pipette and the other trapped and held by laser. We are ready to catch a single DNA molecule.

Let's Go Fishing: Catching a Single DNA Molecule

The DNA reservoir is filled with nearly 2 ml of buffer and 2μl of the biotin labeled Λ-DNA (48,500 base pairs) is added. One may think that adding more DNA will enable the DNA trapping process to be easier but having too much DNA in the reservoir will cause havoc in the system. The DNA will aggregate with each other, stick the flow-cell, and saturate the experiment rendering it useless. Therefore, it is important to find the right balance between having enough vs having too much. It is important to be very gentle with the DNA unlike the beads. The DNA should be mixed slowly with the 1 ml pipette assuring no bubbles are put into the reservoir tube.

Using the manual controls for the piezoelectric stage we moved the bead attached to the micropipette tip about 6 μm away from the one in the trap. Then the DNA is flowed into the system, allowing it to bind to the bead in the trap. Once one end of a DNA is attached to the bead in the trap the free end will be floating with the flow. By preforming a series of circular

movements, we can attach the floating end of the DNA to the bead attached to the tip. Resulting in a single DNA molecule between the two beads (Figure 29). Once a single DNA molecule is trapped the stray DNA is rinsed by flowing buffer through the flow-cells. We are now ready to stretch the DNA.
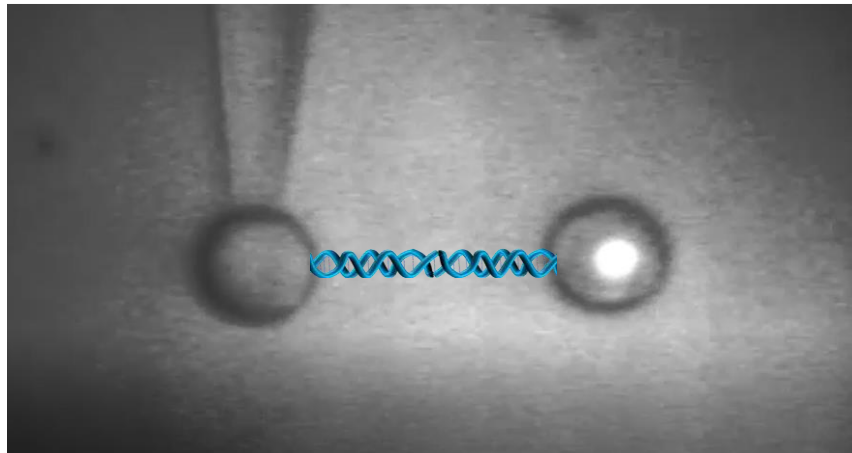
Figure 29: A cartoon DNA (blue) drawn on top of the actual image seen during experiments.

Playing Tug-of-War with DNA

The parameters on our computer program that controls the data collection are then set to take 100 nm steps and wait for 75 ms after each step to collect 1000 data points from the diode detector at each step. Based on the initial point the total number of steps is also given to the program so that the DNA can stretch through the entire melting transition. As the bead on the micropipette tip is moved away from the trap (to the left in Figure 29), the bead in the trap will slightly move (to the left) as well indicating there is a DNA molecule between the two. In real experiments we won't be able to see the DNA but I have drawn a cartoon DNA in Figure 29 to make it easy to visualize. As the bead in the trap shifts due to being pulled by the DNA, the laser deflection is measured by the diode sensors. The stretching curve produced is checked with the

standard DNA stretching curve (shown in the introduction, Figure 11). If it does not match that means it is not a good piece of DNA, thus unusable for an experiment. In the unusable case, the system would then be flushed with buffer and air from the syringe. We then would then start the experiment from scratch beginning with placing the flow-cell into the stage clips. We analyze this curve based upon two models: worm like chain and freely jointed chain model that are discussed in appendix 2.

Stretch and Release Experiments with DOXO

Once we have a good single DNA molecule attached between the beads, we are ready for our real experiments. The concentration of Doxo is made to make a 2 ml solution with buffer within the drug reservoir. Then 1 ml of this drug solution was allowed to flow through the flow-cell before the flow was turned off. This was to assure that the flow-cell chamber was filled with our desired concentration of Doxo. The DNA is then stretched and released by keeping the same parameters used to stretch the DNA without drug (100 nm step size with a 75 ms wait time at each step, averaging a 1000 data points at each point). This procedure was repeated at several concentrations and at least 3 times for each concentration of Doxo to check the reproducibility (shown in the results section). From the literature study, we believed that Doxo should behave as a classical intercalator, that means it would bind and unbind to the DNA in microsecond time scale. If true, the stretching and releasing of the DNA in the presence of Doxo should have overlapped each other, meaning it is in equilibrium, and we should not see any type of hysteresis. But to our surprise we saw hysteresis which became even more prominent as the Doxo

concentration was increased (data shown in Results section).The fact that the stretch and release curves do not overlap can be attributed to Doxo needing an extended period of time to bind and unbind the DNA. To test this hypothesis, we switched to a technique called constant force experiments.

Constant Force Experiments

Constant force experiments is a type of experiment that is designed to stretch and hold the DNA at a constant force while allowing the drug binding to reaching an equilibrium. Initially the DNA is stretched quickly until it reaches the desired force that the user inputs into the program. As the drug binds to the DNA, it obviously will extend the DNA and cause a slack which in turn creates a slight drop in force. In the constant force experiment the program is designed to counter act this decrease in force by stretching the DNA further. The program is created using a force feedback loop capable of holding the DNA to the desired force with the precision of 1 pN (this value is deemed force threshold and can be changed). This allows for us to collect data that describes the extension of the DNA as a function of time in the presence of Doxo at the desired force (data shown in Results section). These experiments unlike the stretch and release would take up to 30 minutes to complete. Apart from the parameters discussed already (step size, step time, and desired force) we additionally could enter in number of iterations desired. The number of iterations corresponds to how many steps will be taken at the desired force to reach equilibrium, ultimately determining the length of time the experiment took. Unlike the stretch and release experiments Doxo would be continuously flown at a steady rate until the Doxo-DNA

complex reached equilibrium. After we see that the drug-DNA binding has reached equilibrium the drug flow is stopped, and the buffer is flown. This will wash away the drug from the system. Constant Force experiments allows us to quantify the binding kinetics of Doxo to DNA in addition to their binding affinity.

Safety

There was a great deal of training required to before conducting experiments. Proper laser safety, chemical safety, and hazard management trainings were paramount. As a lab member I had to take a short course and pass a safety exam yearly to fulfill the requirements of BSU and Northeastern University.

When working with Doxo safety is paramount. Anti-cancer drugs also affect healthy cells, so any time the drug was in use surgical gloves were used. Streptavidin on the beads, Λ-DNA, and biotin is a vitamin, are labeled as non-hazardous chemicals on SDS data sheets, but again surgical gloves were used at all times handling chemicals to form good habits.

Results

Binding of Doxorubicin in Stretch and Release Experiments

As discussed in the methods section, at the beginning of the project stretch and release experiments were completed for various concentrations between 0.07 nM and 15 nM of Doxo. At each concentration, the experiment was repeated multiple times, each time with a new single DNA molecule. Figure 30a shows the stretch (purple solid curves) and release (purple broken curves) from multiple DNA molecules in the presence of 0.7 nM Doxo is plotted onto a single graph. The DNA stretch and release in the absence of Doxo is represented by the black solid and broken curves respectively. As you can see all stretch-release curves from 6 different DNA
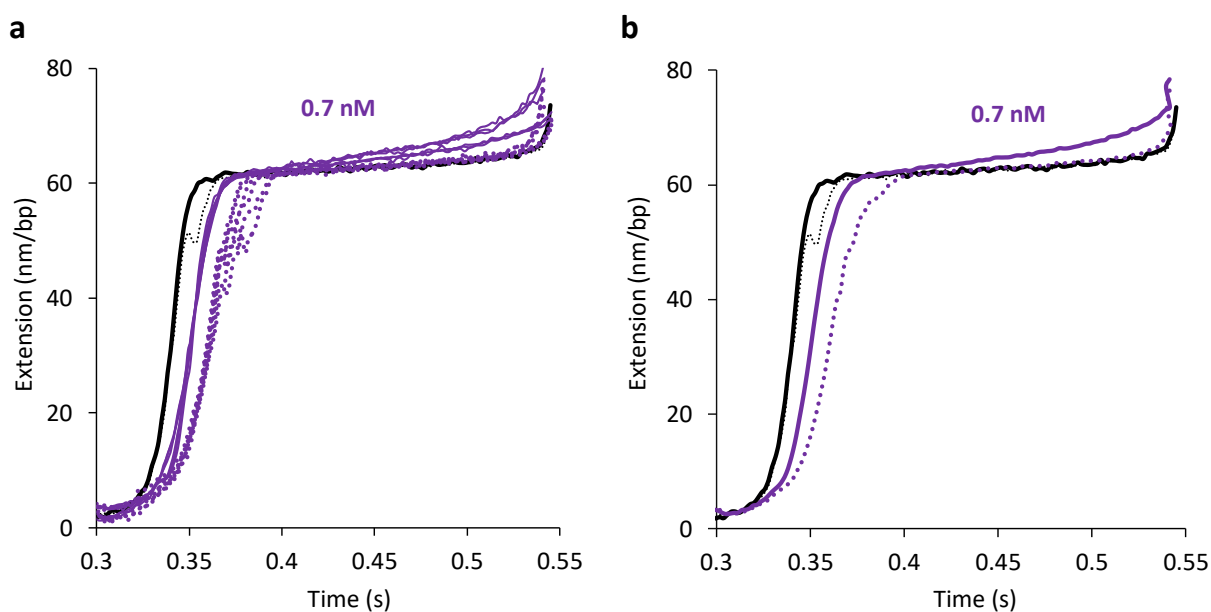
Figure 30: The DNA stretch (solid black curve) and release (broken black curve) is used as reference to compare the stretch (solid purple curve) and release (broken purple curve) curves of DNA molecules in the presence of 0.7 nM Doxo. (a) represents multiple DNA molecules in the presence of Doxo mostly overlapping on top of each other and (b) the average of those DNA molecules, both showing lengthening of DNA and slight increase in the melting transition in the presence of Doxo.

molecules shown in Figure 30a looked pretty similar and almost overlaying on top of each other. Therefore, we averaged them to obtain a single extension vs. time graphs for the 0.7 nM Doxo concentration, which is shown in Figure 30b.

As expected with classical intercalators, in Figure 30 we clearly see that the DNA is extended upon binding to Doxo and a slight increase in melting force during the stretch. But the stretch and release curves of the DNA in the presence of Doxo clearly do not overlap. As discussed previously, in the introduction and in the methods, the stretching of DNA is a reversible process where it should reanneal on the return. When in the presence of a classical intercalator, the DNA-drug complex should equilibrate in the microsecond time scale, thus it should also have overlapping stretch and release curves. The fact that this is not the case means Doxo requires more time to bind completely to the DNA. This behavior is unconventional for a classical intercalators and since almost all literature cites Doxo as classical intercalator we were stumbled upon our first results.

An identical procedure was repeated with 7 nM concentration of Doxo to see whether our results at 0.7 nM make sense. Figure 31 shows the averaged stretch (solid blue) and release (broken blue) curves of multiple experiments where a single DNA molecule was in the presence of 7 nM Doxo. Now we clearly see a huge hysteresis. Also, the lengthening of DNA during the stretch with 7 nM Doxo did not change much from the values we obtained for 0.7 nM Doxo. If Doxo did bind fast to DNA while stretching, with 10-fold higher concentration we should see clear increase in lengthening. But the extensions observed during the return with 7 nM Doxo was definitely greater than that obtained with 0.7 nM Doxo. This supported our previous hypothesis that Doxo needs more time to bind the DNA.
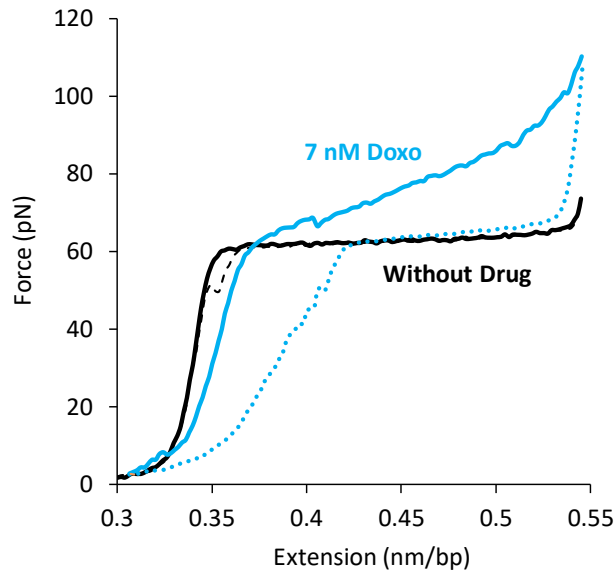
Figure 31: DNA stretch and release curves in the absence of drug (black) and in the presence of 7 nM Doxo (blue) showing increase in the melting transition and clear extension of DNA-Doxo complex during the release. The blue curve is an average of 5 different DNA molecules.

Additionally, in both cases (0.7 nM and 7 nm Doxo concentrations) as the DNA was stretched through the melting transition in the presence of Doxo it resulted in a greater extension of the DNA upon return (represented by the purple and blue dashed lines in Figure 30b and Figure 31 respectively). This added another piece to the puzzle, whether it means that the DNA needed to melt to get adequate binding of Doxo to DNA, to reach the equilibrium state. Classical Intercalators do not require the melting of the base pairs in DNA to bind typically, this made our results go against a well believed trend for a drug that has been studied since the 1970s. We continued the same experiments at various concentrations above and below our initial 0.7 nM Doxo concentration. Interestingly all our experiments followed the same pattern as discussed above.

The plot of release curve averages obtained at various concentrations (figure 32) exhibited classical intercalator behavior. Both the lengthening and melting force of the DNA increased with Doxo concentration. But the main difference being we observe this in the release curves not in the stretching curves as observed for all other classical intercalators [53,54,56]. As mentioned earlier, it can be two factors that cause this. It can be either Doxo is binding slow or it needs the DNA to melt to bind. To explore these features further we switched our experiments from the stretch and release method to the constant force method.
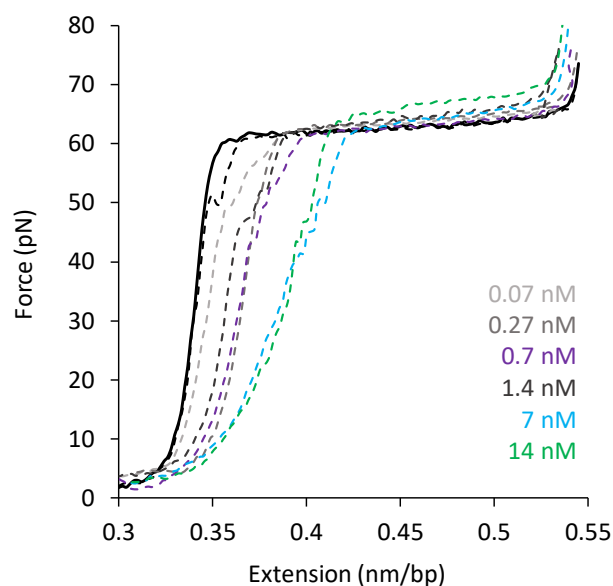
Figure 32: : The average release curves of several concentrations of Doxo (dashed colored) with the DNA stretch and release curves (black) not in the presence of drug used as reference.

Constant force experiments

Through constant force experiments we can stretch the DNA and hold at a constant force (less than the melting force) allowing the drug to reach an equilibrium without going through the melting transition. When the DNA is held at constant force there is a corresponding extension of

the DNA upon the binding of the drug. The DNA-drug complex should then increase in length reaching an equilibrium. The final length of the DNA-drug complex is referred to as equilibrium extension (L_{eq}).

Constant force data obtained in the presence of 27 nM Doxo being held at 20 pN is shown in Figure 33a. In these experiments the normal stretch and release curve of the DNA molecule in the absence of the drug (black) is obtained first and then the DNA is stretched to the desired force and the drug is introduced to the system. The extension of the DNA as the drug binds (orange, Figure 33a) is observed.
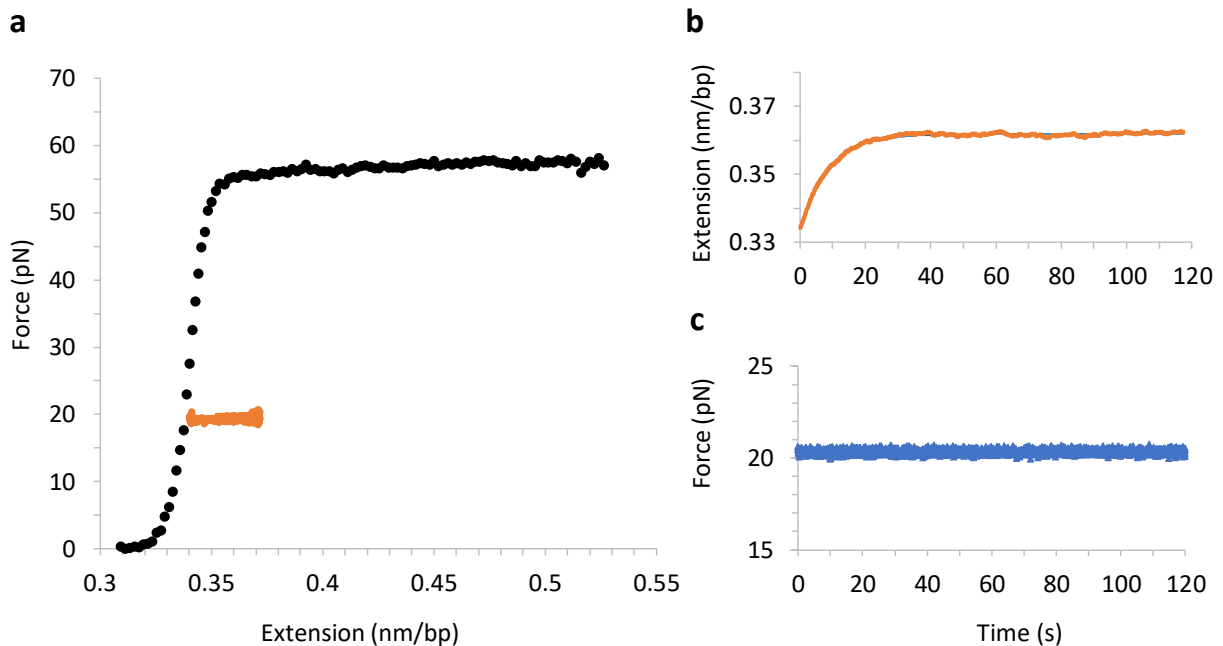
Figure 33: Constant force measurements at 20 pN in the presence of 27 nM Doxo (a) DNA stretching curve (black) in the absence of Doxo and the extension of the DNA that is being held at 20 pN constant force while flowing 27 nM Doxo (orange). (b) the same DNA extension upon the binding of Doxo plotted as a function of time (c) the force measurement while the DNA is being held indicates how well it is maintained as a constant over the duration of the experiment

During the data collection the force and extension are recorded as function of time. Figure 33b

illustrates the plot of extension as a function of time, which clearly shows the DNA elongating,

reaching an equilibrium extension. The plot of force vs time (Figure 33c) assures a constant force

(19.9 ± 0.4 pN) was maintained throughout the experiment.

The extension of the DNA-Doxo complex as a function of time (Data shown in Figure 34) can be

fit to the following equation:

$$L(t) = L_0 + L_{eq}(1 - e^{-k_{tot}t}) \tag{1}$$

Where L_0 refers to the contour length of the DNA without the drug, L_{eq} is the equilibrium

extension of the DNA-Doxo complex, and k_{tot} is the total binding rate of Doxo to the DNA.

Contour length of DNA refers to the length of the DNA molecule at the particular external

stretching force applied. This value can be obtained from the worm like chain model, the

standard dsDNA polymer model (Appendix 2).

Figure 34: The DNA extension upon binding to Doxo while held at constant force 20 pN in the presence
of 27 nM Doxo (open circles) the theoretical fit (solid curve) corresponding to the equation (1)

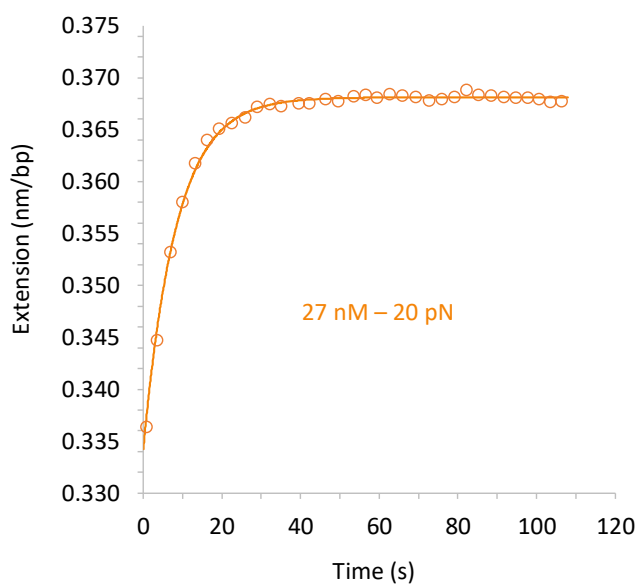The theoretical fit (solid line in Figure 34) for the data (open circles in Figure 34) was obtained based on the equation above by changing two fitting parameters, L_{eq} and k_{tot}. The fitting parameters are automatically varied to minimize the sum of chi-squares using the built-in solver function in Microsoft Excel. A value for chi-square for each data set was estimated by the following equation:

$$\chi^2 = \left[\frac{L_{\text{theoretical}} - L_{\text{experimental}}}{\delta L} \right] \qquad (2)$$

Where, δL is the uncertainty in the measurement of extension.

This procedure was repeated with multiple DNA molecules (5-6) at 20 pN constant force in the presence of 27 nM Doxo to then obtain an average value for L_{eq} and k_{tot}. The standard deviation of the data was recorded as the uncertainty of the measurement.

The overall procedure was repeated at several concentrations at four different constant forces, 20 pN, 30 pN, 40 pN and 50 pN representing the elastic regime of the DNA. Representative data and fittings at several concentrations at these 4 forces are shown in Figure 35.

As seen in the extension vs time plots at all four forces (Figure 35), as the concentration of Doxo is increased the equilibrium extension of the DNA-Doxo complex also increases. Ideally these values of equilibrium extensions obtained from the fitting in the constant force experiments should match that of the release extensions obtained from the stretch and release experiments.

Fortunately, in most cases they do match within the uncertainty, indicating that the release curves were close to equilibrium. Appendix 3 compares the extensions obtained in constant force

measurements and release extensions obtained from stretch and release experiments. The equilibrium extensions obtained in the constant force measurements are used to determine the binding affinity of Doxo intercalating which will be discussed in the next section.
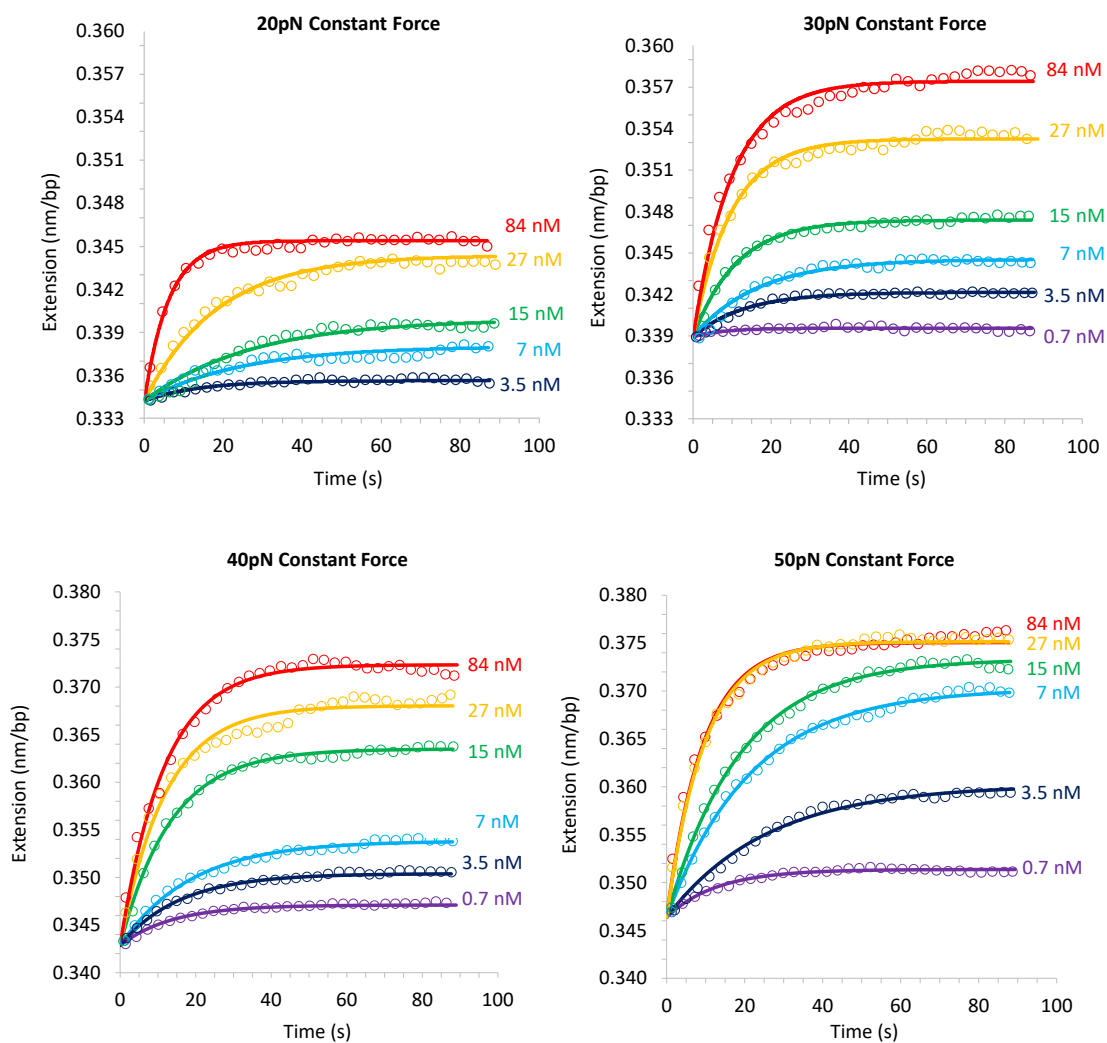

Figure 35: Representative data for the DNA extension as a function of time under the various concentrations of Doxo at the four different constant forces studied. The open circles represent the experimental data averaged while the solid line represents the fit corresponding to equation (1).

Binding Affinity of Doxo

The strength in which a drug binds with the DNA is defined as its binding affinity. In biophysics and biochemistry, the binding affinity is commonly expressed in terms of dissociation constant, K_d, which is the inverse of binding affinity.

To find the dissociation constant first we find the fractional binding of a drug at a certain concentration at the particular force. Using the L_{eq} values from the extension vs. time fittings we can calculate the fractional binding (θ) at particular forces and concentrations with the following expression:

$$\theta(C,F) = \frac{L_{eq}(C,F) - L_0(F)}{\Delta L_{sat}(F)} \tag{3}$$

Where L_0 is the contour length of DNA in the absence of the drug, and ΔL_{sat} is the maximum elongation observed at the particular force when the DNA molecule is saturated with Doxo.

The fractional binding can be used in accordance with a one-dimensional lattice binding model called the McGhee Von Hippel (MGVH) Isotherm[57] to obtain Doxo's dissociation constant at a particular force. Please view appendix 4 for more detail of this model and its applications. The MGVH model provides the following recursive equation that predicts the fractional binding (θ) change with concentration (C) as a function of two important binding parameters, the binding constant (K_d) and the binding site size (n) at a particular force.

$$\theta(K_d,n) = \frac{C}{K_d}\frac{n(1-\theta)^n}{(1-\theta+\frac{\theta}{n})^{n-1}} \tag{5}$$

The fractional binding refers to the fraction of base pairs with ligands bound at equilibrium, compared to the maximum bound at saturation. This means it can only hold a value between 0 and 1. This fitting was done with Microsoft Excel's Data Analysis tool, solver, with fitting parameters K_d and n. But to obtain best K_d values for each data set the value of n was extracted from literature and was set to a value of 1.4. K_d refers to the concentration in which the DNA is 50% saturated with Doxo, henceforth meaning that a low dissociation constant is linked to a high binding affinity.

Figure 36 illustrates an example of MGVH fitting (solid line) and the equilibrium extensions that were used to estimate the fractional bindings (open circles) for various concentrations of Doxo at the 20pN force.
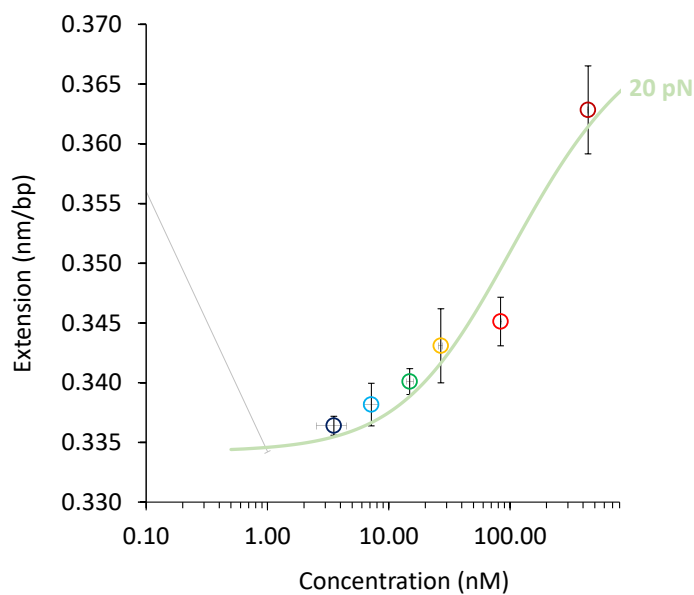
Figure 36: Extension of DNA upon binding to Doxo in the presence of various concentrations of Doxo at 20 pN (open circles) and the best fit to the MGVH isotherm at 20 pN (solid curve).

This procedure of fitting the fractional bindings to MGVH model was repeated at 30, 40, and 50 pN forces to obtain K_d at each force. Figure 37 shows these fittings (solid lines) with the equilibrium extensions that are used to estimate the fractional bindings (open circles) at all four forces that the constant force measurements were done. As mentioned before, each data point is an average measurement from at least 3 separate DNA molecules and the error bars represent the standard deviation.
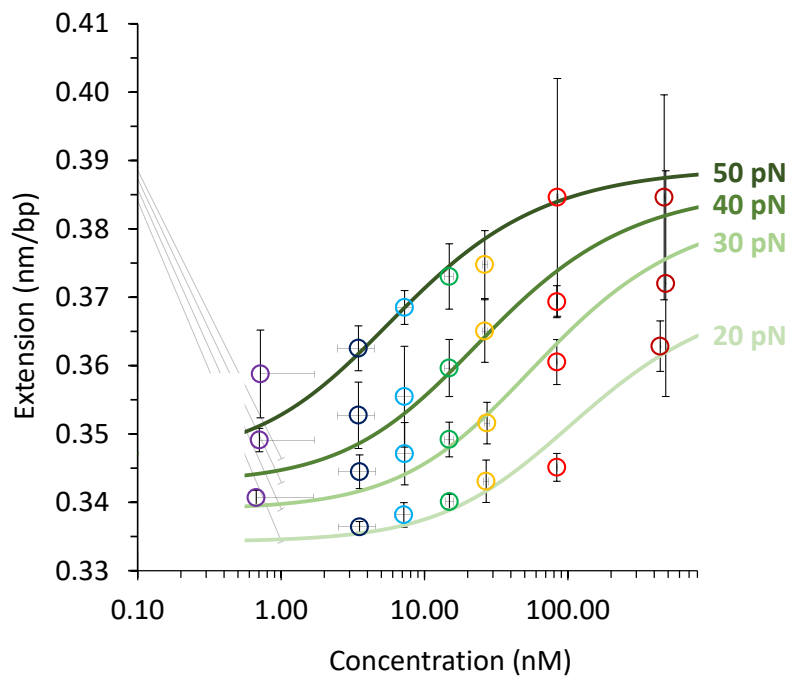
Figure 37: Equilibrium extensions associated with the fractional binding of Doxo at various concentrations at all four forces studied (open circles) and fits to the MGVH isotherms at 20, 30, 40, and 50 pN. Each concentration is color coded with different color.

Force Dependence of Binding Affinity

Once a value of K_d is obtained for all the different forces we can extrapolate its force dependency to obtain a K_d value that is in the absence of force.

Previous single molecule studies[19,22,54,56,58] have shown that the force (F) exponentially facilitates the binding of a drug molecule to the DNA by stretching and extending it by a length Δx_{eq}. This extension is associated with a single intercalation event and in fact the work done to reduce the energy barrier for a single intercalation is represented by $F\Delta x_{eq}$.

This provides us a thermodynamic exponential model:

$$K_d = K_d(0)e^{(\frac{-F\Delta X_{eq}}{k_B T})} \tag{6}$$

Where k_B is Boltzmann's constant and T is the temperature in K (294 K in the case of our lab which yields $k_B T = 4.06$ pNnm). The fitting is done with minimizing χ^2 to find the best fitting values of $K_d(0)$ and Δx_{eq}.

The K_d values were obtained at all the four forces and are represented on the Figure 38 as open blue circles. The exponential force dependency is shown as the broken blue line where the y-axis is on a logarithmic scale.
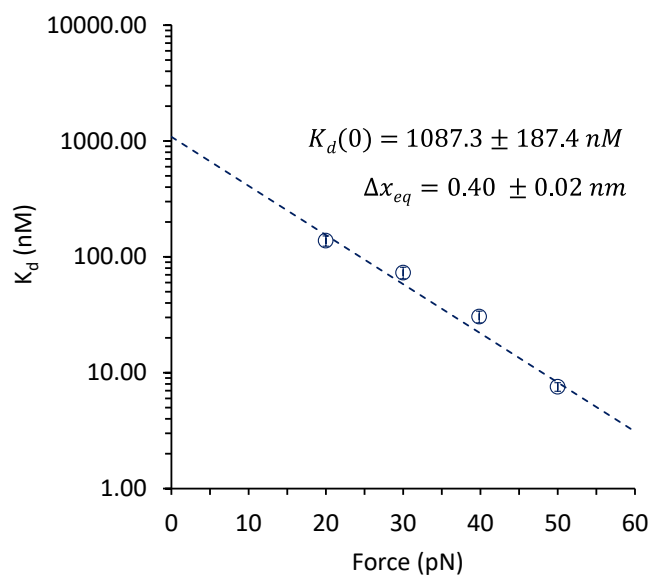
Figure 38: Force dependent analysis of K_d values obtained at various forces using the MGVH fits

(open circles) extrapolated to get the dissociation constant in the absence of force, $K_d(0)$.

The y-axis intercept yields the binding affinity of Doxo in the absence of force, $K_d(0)$ = 1087.3 ± 187.4 nM. The Δx_{eq} value that represents the extension of the DNA per a single intercalation event was determined to be Δx_{eq} = 0.40 ± 0.02 nm. The value of Δx_{eq} obtained for Doxo is comparable to that of the ones obtained for the threading intercalator, Ru-ΛΛ-P studied by Adam Jabak and Nicholas Brydan[19,58]. This value is greater than the other classical intercalators[53,54,56].

Doxo Binding Kinetics (Forthcoming)

The other parameter obtained from the extension vs time fittings of contact force experiments is the total rate, k_{tot}, representing the net binding rate of Doxo to the DNA. It is the addition of both on rate (k_{on}) and off rate (k_{off}). As mentioned in the method section we washed off the

drug after reaching equilibrium and from these experiments we can extract the off rates. By subtracting these off rates from the total rates, we can obtain the on rates.

When the flow is switched from Doxo flow in the experiments to that of the buffer, the buffer will facilitate the unbinding of Doxo and flush the drug away. This will result in the length of the DNA-Doxo complex to decrease from its equilibrium extension. The length decrease can be characterized by an exponential decay equation shown below.

$$L(t) = \left(L_{eq} - L_0\right)e^{-k_{off}t} + L_0 \tag{7}$$

Where L_{eq} is the equilibrium extension at that particular for and concentration, L_0 is the contour length of DNA at that force in the absence of the drug and k_{off} is the off rate. Figure 39 represent an example of washing data (open circles) obtained washing away 27 nM Doxo at 20 pN constant force and the exponential fit (solid line) that is used to obtain the off rate k_{off}.
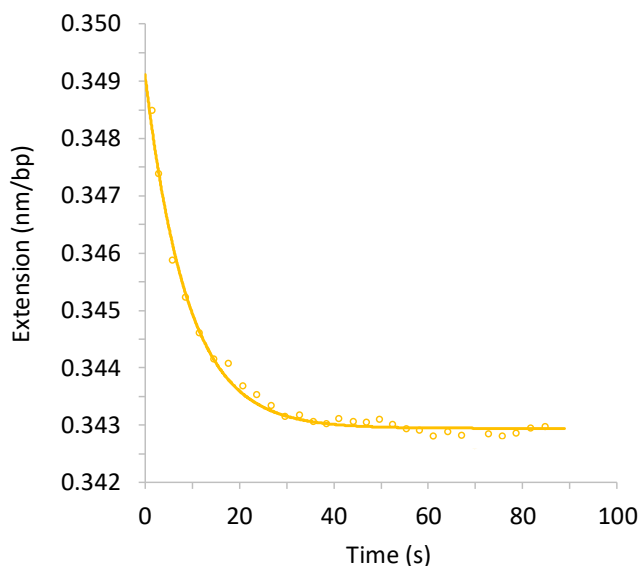
Figure 39: Representative wash data obtained washing away the drug after reaching equilibrium with 27 nM Doxo at 20 pN. The extension of DNA-Doxo (open circles) fitted to equation (7) to obtain the off rate, $k_{off.}$

Once the K_{off} value is obtained, the on rates K_{on} can be extracted through the following expression:

$$K_{tot} = K_{on} + K_{off} \qquad (8)$$

Unfortunately, we are not done with completing the analysis of the washing experiments. This analysis will be completed and included in the manuscript we are planning on writing.

Supplemental Experiments

The biggest question still out there is the extensions that we get during the release curves in the stretch and release experiments showing similar values as constant force experiments. Does this suggest that the melting somehow facilitates the binding of Doxo? If that is the case, can we still characterize Doxo as a classical intercalator? To explore this fact our theoretical collaborator suggested returning to the stretch and release experiments at a slower pace. The idea behind this is to provide the drug enough time to reach equilibrium during each step of the process. During the normal stretch and release the DNA is stretched with a 100 nm step size and after each step a delay of 75 ms is given. This is to accommodate the time to collect 1000 data points and average at each step. To facilitate Doxo binding to reach equilibrium at each step, this step delay was increased to 60000 ms, hence calling it a delayed stretching experiment. These delayed stretches would only go through the elastic regime because of the time it takes to conduct one stretch and release experiment. Although we have done some preliminary experiments, we need to do more data analysis and data acquisition to confirm any trend.

Discussions

Doxo is one of the most prominently used cancer therapeutics yet the mechanism by which it binds at the molecular level is left largely uncharacterized. One prominent way to prevent cancer progression is halting DNA replication. In the study, which we have conducted over the past four years we have investigated the way in which Doxo binds to the DNA at the single molecule level.

Based on Doxo's structure and previous studies it is believed to behave as a classical intercalator but our study challenges that notion with clear evidence. Doxo does not only need an extended amount of time to bind to DNA but it also seems that the DNA melting also facilitates its binding. One way to test whether melting is facilitating the equilibrium is to do delayed stretch experiments as discussed in the results section. In these experiments after each 100 nm step we take with the DNA we wait for almost a minute to provide enough time to reach equilibrium along the stretch. We started these experiments but need more data to confirm what is happening.

The equilibrium DNA extension upon one intercalation event, Δx_{eq}= 0.40 ± 0.02 nm, is pretty high compared to other classical intercalators studied. Other classical intercalators such as Ethidium, and Oxazole Yellow (YO) have Δx_{eq} values of 0.25 ± 0.03 nm and 0.23 ± 0.01 nm respectively[56]. On the other hand, the Δx_{eq} value for Doxo is comparable to the extensions obtained with threading intercalators. Threading intercalators such as Thiocoraline, and $(\Delta,\Delta - Pc)^{+4}$ have Δx_{eq} values of 0.41 ± 0.01 nm and 0.44 ± 0.04 nm respectively[56]. Exemplifying the fact that, the length extension of many classical intercalators is much less than that of Doxo. Our hypothesis from this is that Doxo could possibly be forming dimers before binding at the

micromolar concentration as well, not only the millimolar range as previously described. Further, the positively charged Doxo in solution could be interacting with the negatively charged backbone of the DNA which leads to groove binding. This could create a two-state binding mechanism of Doxo to DNA. The analysis that we have done is based upon single state binding. If there are two states involved, we have to reconsider the fitting models and rethink on how proceed further. This becomes a bigger challenge because there are no standards established yet to analyze groove binders with optical tweezers. Although there are handful of studies that have been done at low forces to characterize groove binding, it has not been completely characterized through higher forces at the single molecule level.

Moving forward, the very first thing to do is to continue the preliminary data acquisition of the delayed stretch experiments and see if it matches that of the constant force experiments. If it does then we have characterized Doxo's binding to the DNA at high forces for the first time, obtaining binding kinetics and affinity. This would be the first study of such and furthermore of a classical intercalator behaving as a threading intercalator.

Appendix 1: Recognizing DNA as the Genetic Material

In 1859 a famous scientist by the name of Charles Darwin pitched a theory in one of the most famous scientific pieces of all time, "The Origin of Species"[59]. Darwin was attempting to propose his theory of natural selection, where a species will change in small ways causing a population to change over several generations, otherwise known as evolution. He used an example in which he stated that whales could be rendered from a bear if given ample conditions and time[59]. With the explanation being, black bears were known to catch insects by swimming with their mouths open which could be related to whales, which are more aquatic in structure and habitat but carries out a similar function in the water. He later removed this analogy in later editions of his book when the scientific community did not respond the way in which he expected. It was concluded by Darwin that organisms possess the ability to change overtime passing on both physical and behavioral traits to following generations. This would be scrutinized by scientists for years to come and the biggest question raised was: what causes the species to change over time?

Six years later, Gregor Mendel was studying pea and fuchsias plants in his botanical garden within the capitol of Austria, Vienna, to understand the question posed from Darwin's theory. Mendel's experiments[60] with these plants went unrecognized for many years by others not utterly understanding its significance. His work introduced the world to proteins, modern genetics, and describe the principles of heredity[61].

In 1869, a few hundred miles North into Germany at the Felix Hoppe-Seyler Laboratory (figure A1)[62], a Swiss doctor named Friedrich Miescher studied leukocytes (white blood cells). He was trying to understand proteins and their functions through a chemical isolation experiment.

During these experiments, he stumbled upon a novel substance that was neither that of a protein or a lipid, what he called "nuclein"[63].

Figure A1: The kitchen of the Tubingen castle where Miescher worked
on his discovery of DNA. This room formed part of the Hoppe-Seyler's
Lab. Photo was taken by Paul Sinner in 1879

For the years to come Miescher's finding of nuclein (the mixture of nucleic acids and associated proteins) was disregarded and null to the idea that it could hold genetic material. Scientists believed it was far too simple to hold all the information of our genome thus proteins continued to be the accepted genetic material. (Now scientist give credit to Miescher as the one who discovered DNA). Between 1885 and 1901, Albrecht Kossel discovered that DNA composed of four bases; adenine (A), cytosine (C), guanine (G), thymine (T) whose chemical structures can be seen in figure 1[10].

Phoebus Levene, who worked with Kossel continued to work on understanding the DNA structure. He discovered that DNA is a long chain molecule that was made up of three components; a phosphate, a pentose (five carbon) sugar named deoxyribose, and one of the four nitrogenous bases (A, T, C, G). Levene stated that the bonding of the three groups would form what is called a nucleotide[64]. But he incorrectly proposed the tetranucleotide structure, where 4 of these nucleotides form a small circular molecule, which then repeats to form the long chain molecule. Based on the structure he proposed Levene believed that the DNA cannot be the genetic material and sided with those who believed protein as the genetic material.

In 1928 Frederick Griffith would return to the notion of DNA being involved in inheritance. Griffiths' experiments in Liverpool investigated the way in which two strains of bacterium affected the lives of mice[65]. To conclude the experiment in looking at the effect of the different bacterium on the lives of the mice he introduced the theory of competence and a transformation principal[66]. The community took this rather haphazardly not fully adopting it until 1944 when Oswald Avery confirmed Griffiths' hypothesis and research stating that this transforming substance was the genetic material of the cell, or DNA[67].

Appendix 2: Polymer Models describing the dsDNA and ssDNA

The standard DNA stretching curve obtained while stretching dsDNA that is free to rotate is believed to go through a phase transition around 65 pN (Figure A2). This transition is known as force induced melting transition, where the dsDNA is converted into mostly ssDNA. The polymer models, the Worm-Like Chain (WLC) model (green) that describes the dsDNA and the Freely Jointed Chain (FJC) Model that describes ssDNA (blue) is also shown in the plot. These models validates that the transition at 65 pN is the where dsDNA is converted into ssDNA.
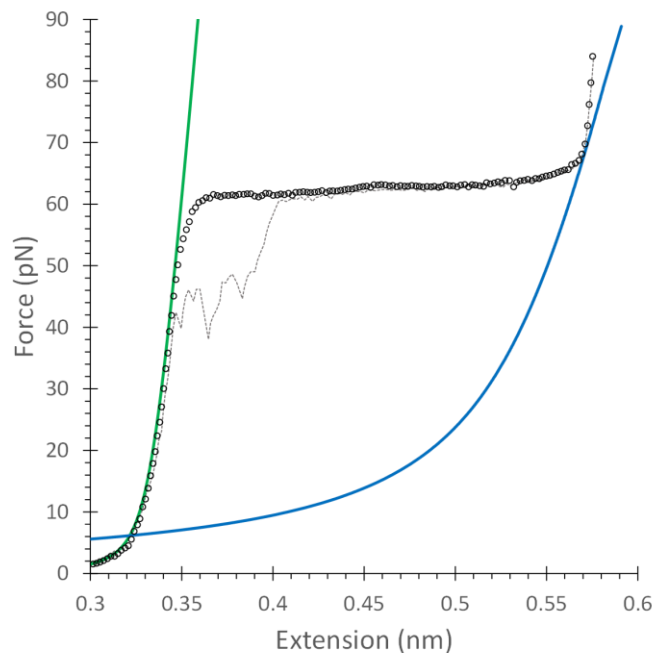

Figure A2: DNA stretch (black solid) and release (black dashed) are shown along with the worm-like chain model (green) that describes dsDNA and freely jointed chain model (blue) that describes ssDNA

Worm Like Chain Model

In 1994 it was shown that the force versus extension curve of a dsDNA molecule can be modeled after the modified worm-like chain (WLC) model[68], a polymer model that is used to describe semi-rigid polymers.

In regard to small pN forces, between that of 0.01 and 10pN, DNA will act as an entropic spring where the WLC model can accurately describe the DNA by assuming smooth distribution of bonding angles. The model describes the force (F) observed within the DNA with particular contour length L_0 when the it is extended by an extension (x):

$$\frac{FP}{k_\mathrm{B}T} = \frac{1}{4}\left(1 - \frac{x}{L_0}\right)^{-2} - \frac{1}{4} + \frac{x}{L_0}$$

Where the contour length broadly defines the length of the molecule when it is at the maximum length without being stretched, k_B is the Boltzmann constant, T is the temperature and P is the persistence length that describes the flexibility of the molecule.

As the DNA is stretched beyond its contour length under higher forces the approximate solution for the extension can be mathematically represented as[18]:

$$x = L_0\left[1 - \frac{1}{2}\left(\frac{K_\mathrm{b}T}{FP}\right)^{\frac{1}{2}} + \frac{F}{S}\right]$$

Where S is the elastic stretching modulus accounting for how the backbone of the molecule extends.

Freely Jointed Chain Model

Double stranded DNA (dsDNA) has a more rigid structure than that of single stranded DNA (ssDNA) due to the base pairing and stacking interactions within the molecule. This in turns makes for a more rigid molecule overall in the dsDNA form compared to that of the ssDNA. Unlike that of the WLC the Freely Jointed Chain Model (FJC) breaks down the molecule into individual parts, monomers if you will, what can be connected freely through wide range of bond angles like jointed chains.

An expression for the observable length of ssDNA under a force (F); this can be written as[18]:

$$z = L_{0.ss}\left[\coth\left(\frac{2P_{ss}F}{k_BT}\right) - \frac{1}{2}\left(\frac{k_BT}{P_{ss}F}\right)\right]\left[1 + \frac{F}{P_{ss}}\right]$$

Where z represents the length of the ssDNA being stretched, $L_{0,ss}$, and P_{ss} are the contour and persistence lengths of ssDNA.

Appendix 3: Constant Force Vs Stretch and Release

We did stretch and release of the DNA to different positions with respect to the melting transition in the presence of 15 nM Doxo to understand whether the melting facilitates the binding.

Table 1: The average stretching length from these experiments at each point in the melting transition (MT) are compared with that of the equilibrium extensions obtained from constant force measurements.

Force	Stretch and Release Before MT	Stretch and Release up to the Beginning of MT	Stretch and Release up to the Midpoint of MT	Stretch and Release up to the End of MT	Constant Force Measurement
(pN)	(nm)	(nm)	(nm)	(nm)	(nm)
20	0.336 ± 0.003	0.351 ± 0.017	0.357 ± 0.014	0.350 ± 0.011	0.340 ± 0.001
30	0.342 ± 0.003	0.358 ± 0.018	0.367 ± 0.013	0.356 ± 0.013	0.349 ± 0.003
40	0.348 ± 0.003	0.365 ± 0.020	0.376 ± 0.013	0.362 ± 0.017	0.360 ± 0.004
50	0.357 ± 0.005	0.371 ± 0.021	0.384 ± 0.014	0.370 ± 0.013	0.375 ± 0.006

It is clear that stretch and release before reaching the melting transition (blue column) has the lowest extension at every force indicating very little Doxo binding. But progressively stretching into the transition (green and yellow column) increases the extension indicating more Doxo binding at all four forces. But once you start stretching to the end of the transition (red column) the extension shrinks back a little bit at all four forces.

The values obtained with stretch and release through the entire melting transition is similar to the equilibrium extension value obtained in the constant force measurements (grey column) within uncertainties at all four forces.

Appendix 4: McGhee Von-Hippel Isotherm Model

In 1974 James McGhee and Peter Von-Hippel created the elegant analytical expression for the isotherm describing how a ligand can bind to a lattice like structure. The McGhee Von-Hippel (MGVH) Model used three parameters, (1) Intrinsic binding constant, K, (2) Unitless cooperative parameter, w, and (3) number of lattice sites covered by a ligand, n to characterize number of ligands bound per lattice site. Conditional probabilities were used to obtain the original McGhee and Von Hippel formula:

$$\frac{v}{L} = Kw(1 - nv)\frac{1 + (2w - n - 1)v + Q}{(2w - 1)(1 - nv) + v + Q}\left[\frac{2w(1 - nv)}{(2w - 1)(1 - nv) + v + Q}\right]$$

Where, $Q = \sqrt{(1 - (n + 1)v^2) + 4wv(1 - nv)}$

Furthermore, v is the number of bound ligands per lattice site holding a value between 0 and 1/n.

For the experiments in which we conduct we use the MGVH isotherm to determine a small molecule's binding affinity at a certain force to DNA which can be thought of as a one-dimensional lattice structure. More simply stated the molecule's binding affinity just means its strength of binding between the ligand (Doxo) and a receptor (DNA), where in parentheses regards our specific experiment.

In particularly we are focused with the one-dimensional homogeneous lattice of DNA, meaning

that non-specific binding of the ligand into the bases of the DNA, which reduces the equation to

a simpler form[20]:

$$\theta(K_d, n) = \frac{C}{K_d} \frac{n(1-\theta)^n}{(1-\theta+\frac{\theta}{n})^{n-1}}$$

Where K_d is the dissociation constant, C is the concentration, θ is the fractional equilibrium

binding, and n is the binding site size.

References

1   Plana, J. C. The red devil revisited. *JACC Cardiovasc Imaging* **6**, 886-888,

         doi:10.1016/j.jcmg.2013.04.009 (2013).

2   Wright, J. Deliver on a promise. *Sci Am* **311**, S12-13 (2014).

3   Arcamone, F. *et al.* Adriamycin, 14-hydroxydaunomycin, a new antitumor antibiotic

         from S. peucetius var. caesius. *Biotechnol Bioeng* **11**, 1101-1110,

         doi:10.1002/bit.260110607 (1969).

4   Minotti, G., Menna, P., Salvatorelli, E., Cairo, G. & Gianni, L. Anthracyclines: molecular

         advances and pharmacologic developments in antitumor activity and cardiotoxicity.

         Pharmacol Rev **56**, 185-229, doi:10.1124/pr.56.2.6 (2004).

5   Johnson-Arbor, K. & Dubey, R. in *StatPearls*   (2020).

6   Wortman, J. E., Lucas, V. S., Jr., Schuster, E., Thiele, D. & Logue, G. L. Sudden death

         during doxorubicin administration. *Cancer* **44**, 1588-1591, doi:10.1002/1097-

         0142(197911)44:5<1588::aid-cncr2820440508>3.0.co;2-x (1979).

7   Siegel, R. L., Miller, K. D. & Jemal, A. Cancer statistics, 2019. *CA Cancer J Clin* **69**, 7-34,

         doi:10.3322/caac.21551 (2019).

8   Roy, P. S. & Saikia, B. J. Cancer and cure: A critical analysis. *Indian J Cancer* **53**, 441-442,

         doi:10.4103/0019-509X.200658 (2016).

9   Fodale, V., Pierobon, M., Liotta, L. & Petricoin, E. Mechanism of cell adaptation: when and how do cancer cells develop chemoresistance? *Cancer J* **17**, 89-95, doi:10.1097/PPO.0b013e318212dd3d (2011).

10   Kossel, A. Nobel Lectures. *Physiology or Medicine 1901 - 1921* (1967).

11   Chargaff, E., Lipshitz, R., Green, C. & Hodes, M. E. The composition of the deoxyribonucleic acid of salmon sperm. *J Biol Chem* **192**, 223-230 (1951).

12   Franklin, R. E. & Gosling, R. G. Evidence for 2-chain helix in crystalline structure of sodium deoxyribonucleate. *Nature* **172**, 156-157, doi:10.1038/172156a0 (1953).

13   Watson, J. D. & Crick, F. H. Molecular structure of nucleic acids; a structure for deoxyribose nucleic acid. *Nature* **171**, 737-738, doi:10.1038/171737a0 (1953).

14   Olins, A. L. & Olins, D. E. Spheroid chromatin units (v bodies). *Science* **183**, 330-332, doi:10.1126/science.183.4122.330 (1974).

15   Thomas, J. O. & Kornberg, R. D. An octamer of histones in chromatin and free in solution. *Proc Natl Acad Sci U S A* **72**, 2626-2630, doi:10.1073/pnas.72.7.2626 (1975).

16   Deweese, J. E. & Osheroff, N. The DNA cleavage reaction of topoisomerase II: wolf in sheep's clothing. *Nucleic Acids Res* **37**, 738-748, doi:10.1093/nar/gkn937 (2009).

17   Alberts, B. DNA replication and recombination. *Nature* **421**, 431-435, doi:10.1038/nature01407 (2003).

18   Chaurasiya, K. R., Paramanathan, T., McCauley, M. J. & Williams, M. C. Biophysical characterization of DNA binding from single molecule force measurements. *Phys Life Rev* **7**, 299-341, doi:10.1016/j.plrev.2010.06.001 (2010).

19   Bryden, N. Quantifying the DNA Binding Properties of the Binuclear Ruthenium Complex Lambda-Lambda-P. *Bridgewater State University* (2016).

20   Almaqwashi, A. A. *et al.* Strong DNA deformation required for extremely slow DNA threading intercalation by a binuclear ruthenium complex. *Nucleic Acids Res* **42**, 11634-11641, doi:10.1093/nar/gku859 (2014).

21   Clark, A. G. *et al.* Reshaping the Energy Landscape Transforms the Mechanism and Binding Kinetics of DNA Threading Intercalation. *Biochemistry*, doi:10.1021/acs.biochem.7b01036 (2018).

22   Paramanathan, T. *et al.* Mechanically manipulating the DNA threading intercalation rate. *J Am Chem Soc* **130**, 3752-3753, doi:10.1021/ja711303p (2008).

23   Giordano, S. H., Lin, Y. L., Kuo, Y. F., Hortobagyi, G. N. & Goodwin, J. S. Decline in the use of anthracyclines for breast cancer. *J Clin Oncol* **30**, 2232-2239, doi:10.1200/JCO.2011.40.1273 (2012).

24   Nabhan, C. *et al.* Disease characteristics, treatment patterns, prognosis, outcomes and lymphoma-related mortality in elderly follicular lymphoma in the United States. *Br J Haematol* **170**, 85-95, doi:10.1111/bjh.13399 (2015).

25   Chihara, D. *et al.* Management strategies and outcomes for very elderly patients with diffuse large B-cell lymphoma. *Cancer* **122**, 3145-3151, doi:10.1002/cncr.30173 (2016).

26   Smith, L. A. *et al.* Cardiotoxicity of anthracycline agents for the treatment of cancer: systematic review and meta-analysis of randomised controlled trials. *BMC Cancer* **10**, 337, doi:10.1186/1471-2407-10-337 (2010).

27   McGowan, J. V. *et al.* Anthracycline Chemotherapy and Cardiotoxicity. *Cardiovasc Drugs Ther* **31**, 63-75, doi:10.1007/s10557-016-6711-0 (2017).

28   Agudelo, D., Bourassa, P., Berube, G. & Tajmir-Riahi, H. A. Review on the binding of anticancer drug doxorubicin with DNA and tRNA: Structural models and antitumor activity. *J Photochem Photobiol B* **158**, 274-279, doi:10.1016/j.jphotobiol.2016.02.032 (2016).

29   Lelle, M. *et al.* Overcoming drug resistance by cell-penetrating peptide-mediated delivery of a doxorubicin dimer with high DNA-binding affinity. *Eur J Med Chem* **130**, 336-345, doi:10.1016/j.ejmech.2017.02.056 (2017).

30   Airoldi, M., Barone, G., Gennaro, G., Giuliani, A. M. & Giustini, M. Interaction of doxorubicin with polynucleotides. A spectroscopic study. *Biochemistry* **53**, 2197-2207, doi:10.1021/bi401687v (2014).

31   Box, V. G. The intercalation of DNA double helices with doxorubicin and nogalamycin. *J Mol Graph Model* **26**, 14-19, doi:10.1016/j.jmgm.2006.09.005 (2007).

32   Frederick, C. A. *et al.* Structural comparison of anticancer drug-DNA complexes: adriamycin and daunomycin. *Biochemistry* **29**, 2538-2549 (1990).

33   Pommier, Y., Leo, E., Zhang, H. & Marchand, C. DNA topoisomerases and their poisoning by anticancer and antibacterial drugs. *Chem Biol* **17**, 421-433, doi:10.1016/j.chembiol.2010.04.012 (2010).

34   Lothstein, L., Israel, M. & Sweatman, T. W. Anthracycline drug targeting: cytoplasmic versus nuclear--a fork in the road. *Drug Resist Updat* **4**, 169-177, doi:10.1054/drup.2001.0201 (2001).

35   E.F. Silva, R. F. B., E.B. Ramos, M.S. Rocha. DNA - Doxorubicin Interaction: New Insights and Peculiarities. *Wiley: Biophysics*, 107, doi:10.1002/bip.22998. (2016).

36   Perez-Arnaiz, C., Busto, N., Leal, J. M. & Garcia, B. New insights into the mechanism of the DNA/doxorubicin interaction. *J Phys Chem B* **118**, 1288-1295, doi:10.1021/jp411429g (2014).

37   Raval, G. *Thermodynamic and Spectroscopic Studies on the Molecular Interaction of Doxorubicin (DOX) with Negatively Charged Polymeric Nanoparticles*, (2012).

38   Yadav, N., Madke, B., Kar, S. & Prasad, K. Liposomal doxorubicin-induced palmoplantar erythrodysthesia syndrome. *Indian Dermatol Online J* **6**, 366-368, doi:10.4103/2229-5178.164488 (2015).

39   Qiao, X. *et al.* Uncoupling DNA damage from chromatin damage to detoxify doxorubicin. *Proc Natl Acad Sci U S A* **117**, 15182-15192, doi:10.1073/pnas.1922072117 (2020).

40   Lei, H., Wang, X. & Wu, C. Early stage intercalation of doxorubicin to DNA fragments observed in molecular dynamics binding simulations. *J Mol Graph Model* **38**, 279-289, doi:10.1016/j.jmgm.2012.05.006 (2012).

41   Fulop, Z., Gref, R. & Loftsson, T. A permeation method for detection of self-aggregation of doxorubicin in aqueous environment. *Int J Pharm* **454**, 559-561, doi:10.1016/j.ijpharm.2013.06.058 (2013).

42   The Nobel Prize in Physics 2018. *The Nobel Prize* (2020).

43   Ashkin, A. Acceleration and trapping of particles by radiation pressure. . *Physicsal Review Letters* **24**, 156 (1970).

44   Chu, S., Bjorkholm, J. E., Ashkin, A. & Cable, A. Experimental observation of optically trapped atoms. *Phys Rev Lett* **57**, 314-317, doi:10.1103/PhysRevLett.57.314 (1986).

45   The Nobel Prize in Physics 1997. *The Nobel Prize* (1997).

46   Ashkin, A., Dziedzic, J. M. & Yamane, T. Optical trapping and manipulation of single cells using infrared laser beams. *Nature* **330**, 769-771, doi:10.1038/330769a0 (1987).

47   Ashkin, A. & Dziedzic, J. M. Internal cell manipulation using infrared laser traps. *Proc Natl Acad Sci U S A* **86**, 7914-7918, doi:10.1073/pnas.86.20.7914 (1989).

48   Ashkin, A., Schutze, K., Dziedzic, J. M., Euteneuer, U. & Schliwa, M. Force generation of organelle transport measured in vivo by an infrared laser trap. *Nature* **348**, 346-348, doi:10.1038/348346a0 (1990).

49   Wang, M. D., Yin, H., Landick, R., Gelles, J. & Block, S. M. Stretching DNA with optical tweezers. *Biophys J* **72**, 1335-1346, doi:10.1016/S0006-3495(97)78780-0 (1997).

50   Williams, M. C., Rouzina, I. & Bloomfield, V. A. Thermodynamics of DNA interactions from single molecule stretching experiments. *Acc Chem Res* **35**, 159-166, doi:10.1021/ar010045k (2002).

51   Williams, M. C., Wenner, J. R., Rouzina, I. & Bloomfield, V. A. Entropy and heat capacity of DNA melting from temperature dependence of single molecule stretching. *Biophys J* **80**, 1932-1939, doi:10.1016/S0006-3495(01)76163-2 (2001).

52   Gore, J. *et al.* DNA overwinds when stretched. *Nature* **442**, 836-839, doi:10.1038/nature04974 (2006).

53   Vladescu, I. D., McCauley, M. J., Nunez, M. E., Rouzina, I. & Williams, M. C. Quantifying force-dependent and zero-force DNA intercalation by single-molecule stretching. *Nat Methods* **4**, 517-522, doi:10.1038/nmeth1044 (2007).

54   Vladescu, I. D., McCauley, M. J., Rouzina, I. & Williams, M. C. Mapping the phase diagram of single DNA molecule force-induced melting in the presence of ethidium. *Phys Rev Lett* **95**, 158102, doi:10.1103/PhysRevLett.95.158102 (2005).

55   Daudelin, B. Advanced Dual Beam Optical Tweezers for Undergraduate Biophysics Research. *Bridgewater State University* (2016).

56   Almaqwashi, A. A., Paramanathan, T., Rouzina, I. & Williams, M. C. Mechanisms of small molecule-DNA interactions probed by single-molecule force spectroscopy. *Nucleic Acids Res* **44**, 3971-3988, doi:10.1093/nar/gkw237 (2016).

57   McGhee, J. D. & von Hippel, P. H. Theoretical aspects of DNA-protein interactions: co-operative and non-co-operative binding of large ligands to a one-dimensional homogeneous lattice. *J Mol Biol* **86**, 469-489, doi:10.1016/0022-2836(74)90031-x (1974).

58   Jabak, A. The Effect of Chirality on DNA Threading: Exploring Biuclear Ruthenium Intercalators Using Optical Tweezers. *Bridgewater State University* (2020).

59   Darwin, C. Darwinism. *Ind Med Gaz* **7**, 47 (1872).

60   Mendel, W. B. a. G. Mendel's Principles of Heredity. *Cambridge University Press* (1913).

61   Oldroyd, D. Gregor Mendel: founding-father of modern genetics? *Endeavour* **8**, 29-31, doi:10.1016/0160-9327(84)90126-1 (1984).

62   Dahm, R. From discovering to understanding. Friedrich Miescher's attempts to uncover the function of DNA. *EMBO Rep* **11**, 153-160, doi:10.1038/embor.2010.14 (2010).

63   Dahm, R. Discovering DNA: Friedrich Miescher and the early years of nucleic acid research. *Hum Genet* **122**, 565-581, doi:10.1007/s00439-007-0433-0 (2008).

64   Levene, P. A. & London, E. J. On the Structure of Thymonucleic Acid. *Science* **68**, 572-573, doi:10.1126/science.68.1771.572-a (1928).

65   Griffith, F. The Significance of Pneumococcal Types. *J Hyg (Lond)* **27**, 113-159, doi:10.1017/s0022172400031879 (1928).

66   Blokesch, M. Natural competence for transformation. *Curr Biol* **26**, 3255, doi:10.1016/j.cub.2016.11.023 (2016).

67   Avery, O. T., Macleod, C. M. & McCarty, M. Studies on the Chemical Nature of the Substance Inducing Transformation of Pneumococcal Types : Induction of Transformation by a Desoxyribonucleic Acid Fraction Isolated from Pneumococcus Type Iii. *J Exp Med* **79**, 137-158, doi:10.1084/jem.79.2.137 (1944).

68   Bustamante, C., Marko, J. F., Siggia, E. D. & Smith, S. Entropic elasticity of lambda-phage DNA. *Science* **265**, 1599-1600, doi:10.1126/science.8079175 (1994).